

## Antibiotic capture by bacterial lipocalins uncovers an extracellular mechanism of intrinsic antibiotic resistance

El-Halfawy, O. M., Klett, J., Ingram, R. J., Loutet, S. A., Murphy, M. E. P., Martín-Santamaría, S., & Valvano, M. A. (2017). Antibiotic capture by bacterial lipocalins uncovers an extracellular mechanism of intrinsic antibiotic resistance. *mBio*.

**Published in:**  
*mBio*

**Document Version:**  
Peer reviewed version

**Queen's University Belfast - Research Portal:**  
[Link to publication record in Queen's University Belfast Research Portal](#)

### **Publisher rights**

© 2017 The Authors. This is an open access article published under a Creative Commons Attribution License (<https://creativecommons.org/licenses/by/4.0/>), which permits unrestricted use, distribution and reproduction in any medium, provided the author and source are cited.

### **General rights**

Copyright for the publications made accessible via the Queen's University Belfast Research Portal is retained by the author(s) and / or other copyright owners and it is a condition of accessing these publications that users recognise and abide by the legal requirements associated with these rights.

### **Take down policy**

The Research Portal is Queen's institutional repository that provides access to Queen's research output. Every effort has been made to ensure that content in the Research Portal does not infringe any person's rights, or applicable UK laws. If you discover content in the Research Portal that you believe breaches copyright or violates any law, please contact [openaccess@qub.ac.uk](mailto:openaccess@qub.ac.uk).

1  
2  
3  
4  
5  
6  
7  
8  
9  
10  
11  
12  
13  
14  
15  
16  
17  
18  
19  
20  
21  
22  
23  
24

Antibiotic capture by bacterial lipocalins uncovers an extracellular mechanism of intrinsic  
antibiotic resistance

Omar M. El-Halfawy<sup>a,b</sup>, Javier Klett<sup>c</sup>, Rebecca J. Ingram<sup>d</sup>, Slade A. Loutet<sup>e</sup>, Michael E. P.  
Murphy<sup>e</sup>, Sonsoles Martín-Santamaría<sup>c</sup>, and Miguel A. Valvano<sup>a,d</sup>

<sup>a</sup>Department of Microbiology and Immunology, University of Western Ontario, London,  
Ontario, N6A 5C1, Canada; <sup>b</sup> Microbiology and Immunology Department, Faculty of Pharmacy,  
Alexandria University, Egypt; <sup>c</sup> Department of Chemical and Physical Biology, Centre for  
Biological Research, CIB-CSIC, Madrid 28040, Spain; <sup>d</sup> Centre for Experimental Medicine,  
Queen's University Belfast, BT9 7BL, United Kingdom; <sup>e</sup> Department of Microbiology and  
Immunology, University of British Columbia, Vancouver, BC, V6T 1Z3, Canada

Address correspondence to Miguel A. Valvano, [m.valvano@qub.ac.uk](mailto:m.valvano@qub.ac.uk).

Running title: Extracellular antibiotic capture by bacteria

25 **ABSTRACT** The potential for microbes to overcome antibiotics from different classes before  
26 they reach the bacterial cells is largely unexplored. Here we show that a soluble bacterial  
27 lipocalin produced by *Burkholderia cenocepacia* upon exposure to sublethal antibiotic  
28 concentrations increases resistance against diverse antibiotics *in vitro* and *in vivo*. These  
29 phenotypes were recapitulated by heterologous expression in *B. cenocepacia* of lipocalin genes  
30 from *Pseudomonas aeruginosa*, *Mycobacterium tuberculosis* and methicillin-resistant  
31 *Staphylococcus aureus*. Purified lipocalin bound different classes of bactericidal antibiotics and  
32 contributed to bacterial survival *in vivo*. Experimental and X-ray crystal structure-guided  
33 computational studies revealed that lipocalins counteract antibiotic action by capturing  
34 antibiotics in the extracellular space. We also demonstrated that fat-soluble vitamins prevent  
35 antibiotic capture by binding bacterial lipocalin with higher affinity than antibiotics. Therefore,  
36 bacterial lipocalins contribute to antimicrobial resistance by capturing diverse antibiotics in the  
37 extracellular space at the site of infection, which can be counteracted by known vitamins.

38  
39 **IMPORTANCE** Current research on antibiotic action and resistance focuses on targeting  
40 essential functions within bacterial cells. We discovered a previously unrecognized mode of  
41 general bacterial antibiotic resistance operating in the extracellular space, which depends on  
42 bacterial protein molecules called lipocalins. These molecules are highly conserved in most  
43 bacteria and have the ability to capture different classes of antibiotics outside bacterial cells. We  
44 also discovered that liposoluble vitamins, such as vitamin E, overcome *in vitro* and *in vivo*  
45 antibiotic resistance mediated by bacterial lipocalins, providing an unexpected new alternative to  
46 combat resistance by using this vitamin or its derivatives as antibiotic adjuvants.

47

48 Treating infections is becoming increasingly difficult since microbes often show intrinsic, high-  
49 level resistance to virtually all clinically approved antibiotics (1). Ineffective microbial killing  
50 and exposure to sublethal antibiotic concentrations elicit adaptive bacterial stress responses  
51 enhancing antibiotic resistance and tolerance (2-7). Much has been learned about antibiotic  
52 resistance mechanisms at the cellular level (8, 9), but whether microbes subvert the action of  
53 antibiotics before they come in contact with the bacterial cells has remained largely unexplored  
54 with the exception of  $\beta$ -lactamases, which are often trapped into released membrane vesicles (10-  
55 13).

56 *Burkholderia cenocepacia* is a highly multidrug resistant, opportunistic Gram-negative  
57 bacterium that causes serious respiratory infections in patients with cystic fibrosis (14). Bacteria  
58 of the genus *Burkholderia* are notorious for their ability to resist the action of multiple classes of  
59 antimicrobials (15), representing an attractive model to understand intrinsic mechanisms of  
60 resistance in opportunistic bacteria. Recently, we showed that in response to sublethal antibiotic  
61 concentrations, *B. cenocepacia* produce and release molecules such as the polyamine putrescine  
62 and YceI, a conserved hypothetical protein of unknown function (16). YceI proteins comprise a  
63 family of bacterial lipocalins (herein abbreviated as BCNs), which are small proteins widely  
64 conserved in Gram-negative and Gram-positive bacteria, but whose physiological role is unclear  
65 (17, 18). In co-culture experiments, *B. cenocepacia* protects *Pseudomonas aeruginosa* from  
66 killing by different bactericidal antibiotics (16). This effect was abrogated in the *B. cenocepacia*  
67 double deletion mutant  $\Delta bcnA-bcnB$  (16), but the individual contribution of each BCN paralog  
68 and their mechanisms remained unknown.

69 Here, we show that secreted BcnA contributes to increased resistance of *B. cenocepacia* to  
70 various classes of antibiotics *in vitro* and *in vivo*. The expression of BCN orthologs from *P.*

71 *aeruginosa*, *Mycobacterium tuberculosis* and methicillin-resistant *Staphylococcus aureus* in *B.*  
72 *cenocepacia*  $\Delta bcnA$  recapitulated this function. Experimental and computational studies revealed  
73 that BCNs bind to a range of antibiotics, thus preventing their antibacterial activity and  
74 contributing to resistance. X-ray crystallography studies of BCN structures, in combination with  
75 docking and MD simulations, have helped us to rationalize plausible binding modes. We also  
76 discovered that fat-soluble vitamins bound BcnA with a higher affinity than antibiotics, enabling  
77 them to outcompete antibiotics. This finding provides a clinically applicable strategy whereby  
78 known vitamins could become antibiotic adjuvants by increasing the concentration of free  
79 antibiotics in the proximity of bacterial cells, thereby boosting their microbicidal activity.

80

## 81 **RESULTS**

82

83 **BcnA is a secreted bacterial lipocalin required for full resistance of *B. cenocepacia* to**  
84 **different classes of antibiotics.** We investigated the role of *B. cenocepacia* BcnA (BCAL3311)  
85 and BcnB (BCAL3310) by constructing individual deletion mutants in their corresponding genes  
86 and assessing bacterial susceptibility to model bactericidal antibiotics representing different  
87 classes including rifamycins (mRNA transcription inhibitors), fluoroquinolones (DNA  
88 replication inhibitors), several  $\beta$ -lactams (cell wall peptidoglycan synthesis inhibitors), and  
89 cationic antimicrobial peptides (cell membrane active agents). The  $\Delta bcnA$  mutant, but not  
90  $\Delta bcnB$ , had increased susceptibility (4-fold MIC reduction) to rifampicin, norfloxacin,  
91 ceftazidime, and the cationic antimicrobial peptide polymyxin B (PmB), and 2-fold MIC  
92 reduction to meropenem. No effect was observed with the aminoglycoside gentamicin (protein  
93 synthesis inhibitor) (Fig. 1A; see antibiotic chemical structures in Fig. S1). Similarly, we also

94 tested model bacteriostatic antibiotics representing different classes. The  $\Delta bcnA$  mutant, but not  
95  $\Delta bcnB$ , had increased susceptibility to minocycline (tetracycline family protein synthesis  
96 inhibitor; 4-fold MIC reduction), and trimethoprim (pyrimidine inhibitor of bacterial  
97 dihydrofolate reductase; 2-fold MIC reduction), while no effect was observed with the macrolide  
98 (protein synthesis inhibitor) azithromycin (Fig. 1A and Fig. S1).

99 The expression of *bcnA* and *bcnB* genes in response to antibiotics at near-MIC (sublethal)  
100 concentrations was characterized by constructing chromosomal *lux* fusions. Expression of  
101 *bcnA::luxCDABE* was upregulated upon exposure to PmB, rifampicin, and norfloxacin, but not  
102 ceftazidime (Fig. 1B). In contrast, *bcnA::luxCDABE* expression was slightly reduced in response  
103 to gentamicin, likely due to protein synthesis inhibition at near-MIC concentrations (Fig. 1B).  
104 Expression of *bcnB::luxCDABE* only increased by exposure to norfloxacin and ceftazidime, and  
105 was slightly reduced by rifampicin and gentamicin (Fig. S2A). Thus, *bcnA* and *bcnB* genes  
106 respond to antibiotic stress, but they appeared to be differentially regulated. *bcnA* and *bcnB* are  
107 located on the same strand and apart by 63 base pairs (Fig. 1C). Immediately upstream of *bcnA*  
108 there is an open reading frame (BCAL3312), also transcribed in the same strand, which encodes  
109 a predicted cytochrome b651 protein. Putative promoter regions are found upstream from  
110 BCAL3312 and downstream from *bcnB* next to a predicted Rho-independent transcription  
111 termination sequence. The genomic organization of the *bcn* region suggest BCAL3312-*bcnA*-  
112 *bcnB* are cotranscribed and may form an operon. However, the transcribed 63-bp intergenetic  
113 region between *bcnA* and *bcnB* has the potential to form strong RNA secondary structures, which  
114 might explain the differential regulation of both genes by antibiotics. The secretion of BcnA and  
115 BcnB proteins was also investigated using FLAG-tagged derivatives; only BcnA was secreted  
116 extracellularly into the growth medium (Fig. S2B). From these experiments, we concluded that

117 BcnA is the major contributor to intrinsic antibiotic resistance upon antibiotic stress and is  
118 secreted to the extracellular bacterial milieu.

119 **BCN orthologs from different species restore BcnA function in *B. cenocepacia*.** To  
120 demonstrate whether BCN orthologs from other bacteria could restore BcnA function in the  
121  $\Delta bcnA$  strain, we tested BCNs of *P. aeruginosa* PAO1 [PA0423, PA4340 and PA4345, herein  
122 BcnA1(Pa), 2 (Pa), and 3(Pa), respectively], *Mycobacterium tuberculosis* H37Rv [Rv1890c,  
123 BcnA(MTb)] and the community-acquired methicillin-resistant *Staphylococcus aureus* USA300  
124 [SAUSA300\_2620, BcnA(Sa)]. CFU counts on PmB-containing plates (Fig. 2A), and Etest  
125 MICs against rifampicin, ceftazidime, and ciprofloxacin (a fluoroquinolone closely related to  
126 norfloxacin) (Fig. 2B) showed that heterologous expression of BCNs from these different  
127 bacteria restores antibiotic resistance to parental levels, indicating these proteins have a  
128 conserved function.

129 **BcnA sequesters antibiotics.** BCNs bind to diverse hydrophobic molecules (19-21); hence  
130 we hypothesized that BCNs could capture antibiotics and reduce their effective concentration in  
131 the bacterial milieu. An antibiotic bioassay demonstrated that BcnA sequestered rifampicin,  
132 PmB, norfloxacin and ceftazidime, in descending order of magnitude, but not gentamicin (Fig.  
133 3A and Fig. S3, A-E). Further, the relative affinity of BcnA for antibiotics was determined *in*  
134 *vitro* by binding competition of antibiotics with Nile Red in complex with BcnA. Nile Red is a  
135 fluorophore used to test hydrophobic binding sites in proteins (22). The calculated binding  
136 inhibitory constants ( $K_i$  values) for each antibiotic (Fig. 3B and Fig. S3, F-M) mirrored their  
137 relative ability to be sequestered by BcnA (Fig. 3A) and the antibiotic susceptibility phenotypes  
138 of  $\Delta bcnA$  (Fig. 1A). Notably, the binding of BcnB to Nile Red occurred at ~20-fold lower  
139 affinity than that of BcnA (Fig. S3, N-Q) agreeing with the lesser role of BcnB in antibiotic

140 resistance. The involvement of hydrophobic moieties in the interaction of ligands with BcnA was  
141 suggested by the significantly higher  $K_i$  value of PmB nonapeptide, which lacks the hydrophobic  
142 N-terminal tail of PmB (23), relative to PmB (Fig. 3B, Fig. S3, F-I). Notably, azithromycin and  
143 gentamicin, the only antibiotics not showing antibiotic sensitivity reduction phenotype with  
144  $\Delta bcnA$  (Fig. 1A), are the only tested antibiotics lacking aromatic or hydrophobic moieties (Fig.  
145 S1). To test polar hydrophilic binding sites in BcnA compared to hydrophobic sites, we used two  
146 related BODIPY dye-labelled phospholipids. BcnA increased the intensity of fluorescence of  
147 BODIPY fluorophore when attached to fatty acyl chain of the phospholipid in BODIPY-  
148 phosphocholine, but not when attached to the hydrophilic polar head group (BODIPY-  
149 phosphoethanolamine) (Fig. S3, R-T). This further supported a role for fatty acyl chains in the  
150 interaction with hydrophobic sites in BcnA.

151 **Structure and molecular modeling reveal distinct docked binding modes for BcnA.** To  
152 elucidate the mode of binding of antibiotics within BCNs, we first solved the X-ray crystal  
153 structures of BcnA and BcnB to 1.4- and 1.6-Å resolution, respectively (*Supplemental Results*,  
154 Table S1 and Fig S4A-E). Visual inspection and structural alignments by the DALI server (24)  
155 confirmed a barrel-shaped lipocalin fold for both proteins (Fig. 4A and B). An octaprenyl  
156 pyrophosphate was bound within a long, hydrophobic tunnel extending from one end of the  
157 barrel in each structure (Fig. S4A and B). The binding of octaprenyl pyrophosphate potentially  
158 occurred during recombinant expression in *Escherichia coli*. Analysis with the PDBePISA server  
159 (25) predicted that BcnA is a monomer whilst BcnB is a dimer by crystallographic symmetry  
160 ( $\sim 2840 \text{ \AA}^2$  of buried surface area including a portion of the tunnel opening). These oligomeric  
161 states were confirmed in solution using size exclusion chromatography-multiangle light  
162 scattering (SEC-MALS, Fig. S4C and D). Superposition of BcnA chain A and BcnB chain C



163 (148 C $\alpha$  atoms, 22% sequence identity) resulted in a root mean squared deviation of 1.66 Å (Fig.  
164 4C). The largest structural differences observed were located in two of the loops that make up  
165 the tunnel opening (Fig. 4C). These differences may play a role in the antibiotic binding potential  
166 of BcnA and BcnB.

167 Using the established crystallographic structures, we applied molecular modeling and  
168 docking calculations to predict BCN binding modes for antibiotics (*Supplemental Results*). These  
169 studies suggested two distinct docked binding modes for BcnA. One binding mode involved  
170 residues in the rim of the lipocalin pocket (Fig. 4D and Fig. S4F-I). Polar interactions, mainly  
171 with polar residues, were observed with all tested antibiotics. There were also interactions  
172 between the aromatic moieties in PmB, rifampicin, norfloxacin, and ceftazidime, and lipophilic  
173 residues. These interactions were not observed with gentamicin, as it lacks aromatic moieties;  
174 that may contribute to weak binding to BcnA. The second binding mode was predicted for more  
175 lipophilic molecules (e.g. Nile Red), occurring deeper inside the lipophilic tunnel (Fig. 4E).  
176 Further, analyses from molecular dynamics (MD) simulations suggested both structural and  
177 ligand recognition roles for residues D82 and D93 (*Supplemental Results*). These residues are  
178 located in the loops at the top of the tunnel opening of BcnA. Site-directed mutagenesis was  
179 performed and the BcnA<sub>D82A-D93A</sub> mutant showed decreased binding affinity for Nile Red (Fig.  
180 S5A-B), which we propose is due to structural changes (*Supplemental Results*, Fig. S6A-E, and  
181 Fig. S7). Docking Nile Red into the BcnA<sub>D82A-D93A</sub> mutant (following the general docking  
182 protocol with the minimized average structure from the ns 2.5 to the ns 5 of the MD simulation)  
183 did not lead to any binding position inside the lipophilic tunnel (Fig. S7). Interestingly, D93 is a  
184 highly conserved residue in the consensus motif of the BCN protein family (Fig. S5C),  
185 exemplified in the alignment of BCN homologs (Fig. S5D). Further, Asp is found in equivalent

186 positions to D82 in homologs of *B. cenocepacia* BcnA. Thus, it is credible that the mode of  
187 interaction between BcnA and antibiotics is common among this large family of conserved  
188 bacterial proteins.

189 **Exogenous BcnA protects different bacterial species from antibiotic killing *in vitro* and**  
190 ***in vivo*.** Since *B. cenocepacia* BcnA is secreted (Fig. S2D), as predicted for most other BCNs, we  
191 therefore hypothesized that exogenous BCNs produced by one bacterial species have the  
192 potential to protect other bacteria from the action of antibiotics including antimicrobial peptides.  
193 This was investigated using purified recombinant BCNs from *B. cenocepacia*. *In vitro* antibiotic  
194 protection assays showed that *P. aeruginosa* PAO1 treated with 1.5  $\mu$ M purified BcnA had  
195 reduced sensitivity to PmB, but not with BcnB (Fig. 5A). In contrast, at 8- to 16-fold lower PmB  
196 concentrations, both proteins protected *Salmonella enterica* Typhi, *Shigella flexneri*,  
197 *Acinetobacter baumannii*, *Acinetobacter lwoffii*, and *Acinetobacter junii* strains (Fig. S7A). This  
198 disparity in the PmB concentrations at which protection by BcnA and BcnB occurs correlates  
199 with their relative affinities to Nile red (Fig. S3N-Q, see above). *In vivo* infections in C57BL/6  
200 mice demonstrated that BcnA protected *P. aeruginosa* Q502, a virulent cystic fibrosis clinical  
201 isolate (26), from PmB killing in an intraperitoneal sepsis model (Fig. 5B). We also employed  
202 the *Galleria mellonella* larvae infection model. The  $\Delta$ *bcnA* and  $\Delta$ *bcnB* mutants had reduced  
203 virulence in *G. mellonella* relative to the parent strain (Fig. S7B). However, significantly lower  
204 numbers of  $\Delta$ *bcnA* bacteria than parental and  $\Delta$ *bcnB* strains were recovered from the hemolymph  
205 of infected larvae at 200 min post-infection (Fig. S6B), suggesting  $\Delta$ *bcnA* bacteria were more  
206 susceptible than  $\Delta$ *bcnB* to larvae's humoral immune response, which is mainly driven by host  
207 antimicrobial peptides (27, 28), mirroring the different *in vitro* susceptibility of  $\Delta$ *bcnA* and  
208  $\Delta$ *bcnB* to PmB. Similarly, infection of BcnA-treated *Galleria mellonella* larvae with *P.*

209 *aeruginosa* PAO1, resulted in more rapid killing of the larvae than control or BcnB-treated  
210 larvae (Fig. 5C). We recovered significantly higher bacterial CFUs from the hemolymph of  
211 BcnA-treated infected larvae (Fig. 5D), suggesting that exogenous BcnA provides a survival  
212 advantage to infecting bacteria. Enhanced bacterial killing of BcnA-treated larvae was also  
213 observed for *Klebsiella pneumoniae*, *A. baumannii*, and *S. aureus* USA300 (Fig. S7C). Together,  
214 the *in vivo* infections results underpin a biological role for BCNs in providing a survival  
215 advantage to infecting bacteria from different species.

216 **Liposoluble vitamins inhibit BcnA-mediated antibiotic capture.** Conceivably, molecules  
217 with superior binding affinity to BCNs than that of antibiotics should prevent BCN mediated  
218 resistance. Since lipophilic moieties are predicted to bind deep within the BCN pocket, we tested  
219 normal dietary hydrophobic supplements, recommended for several patient groups including  
220 cystic fibrosis patients, such as the fat-soluble vitamins  $\alpha$ -tocopherol (vitamin E) and  
221 menaquinone (vitamin K2). Docking of  $\alpha$ -tocopherol showed its alkyl chain buried into the  
222 BcnA tunnel and its cyclic head placed towards the entrance, similar to the Nile Red binding  
223 pose (Fig. 4E). Of note,  $\alpha$ -tocopherol followed by menaquinone exhibited very low  $K_i$  values in  
224 Nile Red displacement assays (~2-4 orders of magnitude lower than the  $K_i$  values of antibiotics),  
225 indicative of their high affinity to BcnA (Fig. 3B). This prompted us to test the BCN-inhibitory  
226 activity of fat-soluble vitamins *in vivo*. Using *G. mellonella* larvae infected with *P. aeruginosa*  
227 PAO1, 10  $\mu$ M of either  $\alpha$ -tocopherol or menaquinone significantly reduced the survival  
228 advantage of *P. aeruginosa* in BcnA-treated larvae (Fig. 6A). This supports the notion that the  
229 protective function of BCN on infecting bacteria can be inhibited *in vivo* (Fig. 6B).

230

231 **DISCUSSION**

232 Lipocalins are an ancient family of small proteins found in all kingdoms of life with the ability to  
233 bind hydrophobic ligands, but with different functions depending on the cell types and organisms  
234 (29, 30). In many cases and particularly in bacteria (17), their function is unclear although BCN  
235 orthologs can be found by data mining in the majority of completed genomes. In this study, we  
236 have demonstrated for the first time that secreted BCNs contribute to antibiotic resistance by  
237 capturing and neutralizing antibiotics in the bacterial milieu. BCNs bind a range of antibiotics  
238 with diverse chemical structures, increasing antibiotic resistance *in vitro* and enhancing bacterial  
239 survival *in vivo*. Our structural work suggests that BCNs have two binding modes. Hydrophobic  
240 molecules like Nile Red and Vitamin E and K2 can bind in the interior of the lipocalin tunnel,  
241 while antibiotic molecules interact with the rim and their binding properties are much weaker.  
242 This suggests that antibiotic binding and scavenging is not a primary function of secreted BCNs  
243 but these proteins may also have other yet undiscovered roles.

244 We propose that the antibiotic binding ability of BCNs becomes particularly relevant under  
245 conditions whereby antibiotics cannot effectively kill bacteria and their presence in sublethal  
246 concentrations elicits protective bacterial stress responses. Exposure to antibiotics triggers  
247 complex and multi-factorial bacterial processes involving changes in regulation, metabolism and  
248 energy generation (31-35). There is a body of evidence indicating that antibiotics at sublethal  
249 concentrations can stimulate the production of reactive oxygen intermediates (36-40), and also  
250 that oxidative stress associated with pathological inflammation reduces the efficacy of antibiotics  
251 (33). The increased *bcnA* transcription upon antibiotic treatment indicates this gene responds to  
252 antibiotic-induced stress. Recent work in the model plant *Arabidopsis thaliana* shows that two  
253 lipocalins that are related to bacterial orthologs have distinct but overlapping functions essential  
254 for protection from lipid peroxidation (41). Further, the mammalian odorant-binding protein, a

255 soluble lipocalin, protected the bacterial cells from hydrogen peroxide-induced stress when  
256 overexpressed in *E. coli* (42), whereas *P. aeruginosa* PAO1 BcnA1(Pa) was overexpressed in  
257 response to hydrogen peroxide and paraquat (43). Donnarumma *et al.* (18) have recently  
258 suggested that the highly conserved *Neisseria* BCN (GNA1030) is a ubiquinone-8 binding  
259 protein. Since ubiquinone-8 is a cofactor mainly involved in the electron transport chain (44) and  
260 with antioxidant properties(45), these authors propose a role for this protein in antioxidant  
261 defense, perhaps by delivering ubiquinone-8 to the bacterial membrane or the periplasmic space.  
262 Ubiquinones are prenylated benzoquinones. Interestingly, the majority of known crystal  
263 structures of bacterial lipocalins including BcnA and BcnB have been solved with octaprenyl-  
264 like molecules bound to the lipocalin tunnel, although it is not certain if the presence of this  
265 molecule corresponds to a physiological substrate or is an artefact associated with the protein  
266 purification prior to crystallization. Therefore, while it may be reasonable to propose that BCNs  
267 could play a role in oxidative stress responses the mechanisms involved remain to be elucidated.

268 In summary, we have uncovered a new bacterial strategy for general antibiotic resistance  
269 operating extracellularly based on BCN-mediated antibiotic capture, which provide bacteria with  
270 a selective advantage to overcome antibiotic toxicity particularly in chronic infections where  
271 antibiotic treatment often fails. Further, we reveal a strategy to disrupt antibiotic capture and  
272 propose liposoluble vitamins as clinically usable BCN inhibitors.

273

## 274 MATERIAL AND METHODS

275 **Strains and reagents.** Table S2 lists bacteria and plasmids used in this study. Bacteria were  
276 grown in LB (supplemented with 0.4% rhamnose when required) at 37°C. *Escherichia coli*  
277 cultures were supplemented as required with the following antibiotics (final concentrations):

278 tetracycline (30 µg/ml), kanamycin (40 µg/ml), and trimethoprim (50 µg/ml). *B. cenocepacia*  
279 cultures were supplemented as required with trimethoprim (100 µg/ml), and tetracycline (100  
280 µg/ml). Antibiotics (Sigma) were diluted in water except for PmB, which was diluted in 0.2%  
281 bovine serum albumin/0.01% glacial acetic acid buffer. Rifampicin was dissolved in dimethyl  
282 sulfoxide (DMSO).

283 **General molecular techniques.** DNA manipulations were performed as previously  
284 described (46). T4 DNA ligase (Roche Diagnostics), Antarctic phosphatase (New England  
285 Biolabs) and restriction endonucleases were used as recommended by the manufacturers.  
286 Transformation of *E. coli* GT115 and DH5α was performed using the calcium chloride method  
287 (47). Mobilization of plasmids into *B. cenocepacia* was conducted by triparental mating (48)  
288 using *E. coli* DH5α carrying the helper plasmid pRK2013 (49). DNA amplification by  
289 polymerase chain reaction (PCR) was performed using a C1000 Thermal cycler (Bio-Rad  
290 Laboratories Ltd., Mississauga, Ontario, Canada) with Taq or HotStar HiFidelity DNA  
291 polymerases (Qiagen) and optimized for each primer pair. DNA sequencing was carried out at  
292 Eurofins, Huntsville, Alabama, USA. The DNA sequences were analyzed with the BLAST  
293 computer program and compared to the sequenced genome of *B. cenocepacia* strain J2315. The  
294 sequence of *S. aureus* gene SAUSA300\_2620 was optimized for *B. cenocepacia* codon usage  
295 and custom synthesized at Eurofins. Cloning, expression, and purification of bacteriocalins was  
296 performed as previously described (16). Transcriptional fusions to *luxCDABE* and the  
297 subsequent luminescence expression assays were performed as previously described (36). For  
298 site-directed mutagenesis, pOE16 was amplified with Pfu polymerase using the appropriate  
299 primer pairs; the PCR products were digested overnight with 1 U *DpnI* at 37°C, and then  
300 introduced into *E. coli* DH5α competent cells by transformation. Transformants were selected on

301 LB agar plates supplemented with kanamycin; amino-acid replacements were confirmed by  
302 DNA sequencing.

303 **Protein analysis and Western Blotting.** Overnight cultures were diluted to OD<sub>600</sub> 0.03 in 30  
304 ml fresh LB medium with or without PmB and incubated for 3.5 h at 37°C, 200 rpm. Following  
305 incubation, cells equivalent to OD<sub>600</sub> ~0.2 were pelleted, resuspended in 30 µl SDS-PAGE  
306 protein loading dye, and boiled to obtain whole cell lysates. Secreted proteins were precipitated  
307 from the supernatant of the rest of the cultures using 10% trichloroacetic acid as previously  
308 described (50). Precipitated proteins were resuspended in Tris buffer, 1 M, pH 7.5. The volume  
309 of protein samples loaded to the 16% SDS-polyacrylamide gel was normalized to the OD<sub>600</sub>  
310 value. After SDS-PAGE, proteins were transferred onto nitrocellulose membranes and the  
311 membranes were blocked overnight at 4°C with Western blocking reagent (Roche Diagnostics,  
312 Laval, QC, Canada) in TBST (50 mM Tris-HCl pH 7.5, 150 mM NaCl, 0.1 % Tween-20). The  
313 primary antibodies, anti-FLAG M2 monoclonal antibody (Sigma) or anti- $\alpha$ -subunit RNA  
314 Polymerase (*E. coli*) (Neoclone, Madison, WI, USA), were diluted to 1:15,000 in TBST and  
315 applied for 1.5 h. Secondary antibody, goat anti-mouse Alexa Fluor 680 IgG antibodies  
316 (Invitrogen), was diluted to 1:15,000 and applied for 1 h. Western blots were developed using  
317 LI-COR Odyssey infrared imaging system (LI-COR Biosciences, Lincoln, NE, USA).

318 **Antibiotic susceptibility testing.** The inoculum of *B. cenocepacia* K56-2, the appropriate  
319 mutants and other bacterial species was prepared by the direct colony suspension method  
320 according to CLSI (51). Cultures of OD<sub>600</sub> of 0.0008 in fresh cation-adjusted MHB with or  
321 without the antibiotic were incubated at 37°C with medium continuous shaking in a Bioscreen C  
322 automated growth curve analyzer (MTX Lab Systems, Vienna, VA, USA). Bacterial growth was  
323 assessed turbidimetrically at 600 nm. Etest strips (AB bioMérieux, Solna, Sweden) were applied

324 to agar plates (17 ml agar in 85 mm Petri dish) inoculated with test bacteria by swabbing  
325 overnight cultures diluted to OD<sub>600</sub> of 0.04; plates were then incubated at 37°C for 24 h.  
326 Alternatively, population analysis profiling (PAP) was performed turbidimetrically or by cfu  
327 counting as previously described (16). For *in vitro* protection assays, *B. cenocepacia*  
328 bacteriocalins were added to LB broth at a final concentration of 1.5 μM.

329 ***In vitro* binding assays.** These assays were performed as previously described (22) with few  
330 modifications. Purified BCNs were prepared in phosphate buffered saline (PBS, pH 7.4).  
331 Phospholipids and Nile Red were prepared in DMSO. The binding of each fluorescent probe to  
332 BCNs was measured by titrating 100 μl of BCNs (1.5 μM) in a flat bottom 96-well microtiter  
333 plate (LUMITRAC 200 White, Greiner bio-one, Monroe, NC, USA) with aliquots of increasing  
334 concentrations of probe until fluorescence intensity reached plateau indicating all binding sites  
335 were occupied. All spectra were corrected for background fluorescence determined from probe  
336 into buffer titrations. Fluorescence was measured using a Cary Eclipse Fluorescence  
337 spectrophotometer (Varian) set at an excitation wavelength ( $\lambda_{ex}$ ) specific for each probe, as  
338 follows: Nile Red (550 nm), and BODIPY phospholipids (500 nm for fatty acyl BODIPY labeled  
339 phosphocholine and 505 nm for head group BODIPY labeled phosphoethanolamine). The  
340 emission spectrum for each probe was collected across the following wavelengths ( $\lambda_{em}$ ): Nile  
341 Red (590–750 nm), and BODIPY phospholipids (510–665 nm). The background-corrected  
342 binding fluorescence with each probe was fitted to a one-site binding model as previously  
343 described for human AGP (22). The equilibrium binding affinity constant for the probe–BCN  
344 complex ( $K_D$ ), the probe concentration needed to achieve a half-maximum binding at  
345 equilibrium, was determined by non-linear least square regression analysis of the binding  
346 isotherms using GraphPad Prism V5.0 software (GraphPad software).



347 For probe displacement experiments, antibiotic solutions and fat-soluble vitamins (prepared  
348 in DMSO) diluted in PBS, pH 7.4 were titrated against BCN–probe complex at a saturating  
349 concentration necessary to obtain the maximum fluorescence when bound. Displacement of  
350 probe was measured as the corresponding decrease in fluorescence upon the progressive increase  
351 of antibiotic concentration. The binding inhibitory constants ( $K_i$ ) for the test compounds were  
352 determined by nonlinear regression analysis using competition-binding equations for one site  
353 binding calculated by GraphPad Prism V5.0 software. The lower the  $K_i$  values, the higher the  
354 affinity of the molecule to BcnA. All fluorometric assays were conducted in duplicate 3  
355 independent times.

356 ***Galleria mellonella* larvae in vivo infection.** These assays were performed as described (52)  
357 with modifications. Overnight cultures were diluted in PBS, pH 7.4 with or without *B.*  
358 *cenoepectica* BCNs at 1.5  $\mu$ M final concentration to OD<sub>600</sub> as follows: *B. cenoepectica* and *P.*  
359 *aeruginosa* PAO1 to 0.00004, *K. pneumoniae* Kpn18 to 0.04, *A. baumannii* AB1 to 0.4 and *S.*  
360 *aureus* USA300 to 0.004. The larvae were injected with 10  $\mu$ l of the bacterial suspensions or  
361 sterile PBS (10 larvae/group in each experiment) using 10  $\mu$ l Microliter syringes (Hamilton). The  
362 larvae were incubated at 30°C and their viability was checked at regular time intervals. In similar  
363 assays, 5 larvae/group were sacrificed at 200 min post-infection and the hemolymph was  
364 extracted as previously described (52). The hemolymph was immediately serially diluted in PBS,  
365 plated on LB agar supplemented with 0.3% cetrinide or 200  $\mu$ g/ml Ampicillin- 25  $\mu$ g/ml PmB to  
366 quantify the cfu of *P. aeruginosa* PAO1 or *B. cenoepectica* respectively recovered from the  
367 infected larvae.

368

369       **Intraperitoneal infection in mice.** A clinical isolate of *Pseudomonas aeruginosa* (strain  
370 Q502) was grown overnight in nutrient broth at 37°C with constant agitation. The bacteria were  
371 centrifuged at 2000 ×g and washed 3 times in sterile endotoxin-free PBS. The bacteria were  
372 resuspended in sterile injection-grade saline and the inoculum adjusted to an optical density of  
373 0.5 (A<sub>550</sub>). Female, adult (8-12-week old) C57BL6 mice were infected intraperitoneally with 100  
374 µl of the bacterial suspension, subsequent growth of the inoculum on nutrient agar demonstrated  
375 that each animal received 10<sup>6</sup> CFU. A sample size of n=6 mice per treatment was used. This was  
376 determined by GraphPad StatMate 2.0 to ensure 80% power to detect statistically significant  
377 effects between antibiotic treated and untreated animals at significance level (alpha) of 0.05,  
378 two-tailed. The actual power was >99%. Mice were selected at random from open stock cages (n  
379 = 10 per cage), ear marked to allow individual identification and then sequentially placed into  
380 treatment groups. During the course of the experiment mice were housed in individually  
381 ventilated cages “IVCs”. This method of assigning animals to groups ensures that there is  
382 approximately equal distribution of mice from different stock cages in each group to minimize  
383 the influence of cage-to-cage variability. At the time of inoculation, the mice were treated with  
384 PmB at the standard pediatric dose of 20,000U/kg (n = 6), PmB and 100 µl of 25 µM BCN (n =  
385 6), BCN only (n = 6), or a saline control (n = 6) by intraperitoneal injection. The individual  
386 components injected into mice were added to the same syringe immediately before the IP  
387 injection. Animals were culled by cervical dislocation 4 h post inoculation. The time point was  
388 selected since by this time point and under the infection conditions the untreated mice reach the  
389 humane end point and need to be culled, as defined within the UK Home Office license under  
390 which the experiments were carried out (PLL 2700). Due to the virulence of the clinical isolate,  
391 the dose of the bacterial inoculum, and because the bacteria are delivered IP, the mice rapidly

392 succumb to the infection. In contrast, those given effective antibiotic treatment rapidly clear the  
393 infection and remain perfectly healthy. The vast divergence in response seen in this model  
394 provides us with the statistical power to robustly assess the microbial response to antibiotic  
395 therapies without requiring the use of a very large numbers of mice per group. We are therefore,  
396 adhering to the reduction principle of the 3Rs. The peritoneal cavity was lavaged with 3.5 mL of  
397 ice-cold sterile endotoxin free PBS and the volume recovered recorded. Serial dilutions of the  
398 lavage fluid were plated onto cetrimide agar; bacterial colonies were counted after 24 hours of  
399 growth at 37°C. Harvesting the samples and quantifying the bacterial burden in the mice was  
400 blinded to the treatment groups. Data were not normally distributed and there was not equal  
401 variance between groups; therefore, a non-parametric Kruskal-Wallis test was used. Mouse  
402 infection experiments carried out were assessed by the Queen's University Belfast animal  
403 welfare and ethical review body (AWERB) committee and conducted under a license issued by  
404 the UK home office under the Animals (scientific procedures) Act 1986, amended 2012.

405 **Antibiotic bioassay.** Antibiotic test solutions with or without 1.5 µM BcnA were incubated  
406 for 30 min at 37°C with rotation. The solutions were filtered through filter units with MWCO 10  
407 KDa by centrifugation at 7500g, at 4°C for 10 min. The concentration of antibiotics in the  
408 filtrates was determined by spotting 5 µl on sterile filter discs placed on agar plates swabbed  
409 with the test bacteria. Petri dishes (15 cm diameter) containing 40 ml LB agar were swabbed  
410 with bacterial suspensions of OD<sub>600</sub> 0.04. The plates were incubated at 37°C for 24 hr. Each  
411 plate included 4 discs containing standard concentrations of the antibiotic alongside the discs  
412 impregnated with test and control antibiotic solutions. *E. coli* DH5α was used for bioassays of  
413 PmB, norfloxacin, ceftazidime and gentamicin and *S. aureus* USA300 for bioassays of  
414 rifampicin. The theoretical disc content of the test antibiotic solutions was 10, 5, 2, 30 and 10 µg

415 for PmB, rifampicin, norfloxacin, ceftazidime and gentamicin respectively. Standard antibiotic  
416 discs contained 2-fold higher, the same amount, 2 and 4-fold lower than the test antibiotic discs.  
417 After incubation, the clear zones of inhibition were measured and the antibiotic concentrations  
418 were determined from standard curves constructed from the standard antibiotic discs.

419 **Structure determination.** BcnA and BcnB was purified by FPLC and concentrated to ~ 20  
420 mg/ml in 20 mM Tris, pH 7.5, 100 mM NaCl (1% DMSO for BcnB) with > 95% purity. Protein  
421 solutions were mixed 1:1 with mother liquor and crystals were grown at room temperature.  
422 BcnA crystals grew with 0.1 M Tris, pH 8.5 and 2.4 M ammonium sulphate (final pH 8.0) as the  
423 mother liquor. BcnB crystals grew with 0.1 M HEPES pH 6.5, 26% PEG 6000 as the mother  
424 liquor. Datasets were collected on beam line 08ID-1 at the Canadian Light Source (53),  
425 integrated using iMOSFLM (54), and scaled with AIMLESS (55) from CCP4. Phases for BcnA  
426 and BcnB were obtained using Phaser.MRage (56) from PHENIX using PDB ID 2FGS and  
427 1WUB, respectively, as the search models. Both structures were initially built with AutoBuild  
428 (57) from PHENIX, and then manually built with Coot (58). The BcnA and BcnB structures  
429 were refined with phenix.refine (59) from PHENIX and REFMAC5 (60) from CCP4,  
430 respectively, with TLS refinement for both. Figures were generated using Pymol, version 1.8  
431 (<https://www.pymol.org/>). Data collection and refinement statistics are provided in Extended  
432 Data Table 1. Size exclusion chromatography-multiangle light scattering (SEC-MALS)  
433 experiments were conducted to assess the oligomeric solution state of BcnA and BcnB as  
434 previously described (61) with proteins diluted to 1 mg/ml in 20 mM Tris, pH 7.5, 100 mM  
435 NaCl.

436

437       **Computational Methods.** All codes can be obtained under License Agreement: AMBER 12  
438 and Amber Tools ([www.ambermd.org](http://www.ambermd.org)), Maestro suite ([www.schrodinger.com](http://www.schrodinger.com)), AutoDock 4.2.2  
439 and AutoDockTools (<http://autodock.scripps.edu>, free software). Amber and Maestro have  
440 Academic fees. We studied the stability of the two X-ray structures for BcnA and BcnB, as well  
441 as the D82A-D93A mutant by molecular dynamic (MD) simulations as implemented in AMBER  
442 12. The initial model of D82A-D93A was built with Amber Tools. Missing hydrogen atoms were  
443 added and protonation state of ionizable groups was computed by using Maestro Protein  
444 Preparation Wizard, version 9.3 (<https://www.schrodinger.com/maestro>). Atom types and  
445 charges were assigned according to AMBER ff10 force field (62). The three molecular systems  
446 were hydrated by using cubic boxes containing explicit TIP3P water molecules extending 10 Å  
447 away from any protein atom for simulating the aqueous environment with the help of Amber  
448 Tools with added counter ions to neutralize the system. Before the MD simulations, the two  
449 systems were equilibrated under the following protocol: initial 8000 steps of steepest descent  
450 minimization, followed by heating of the system with position restrain (force constant of 20 kcal  
451 mol<sup>-1</sup> Å<sup>-2</sup>) for all protein atoms during 10 ps of MD simulation increasing the temperature from  
452 100 K to 300 K plus additional 15 ps at constant temperature of 300 K. Position restrain was  
453 gradually decreased during 100 ps at constant 300 K, until the full system was under no restrains  
454 with constant temperature (300 K) and pressure (1 atm). After equilibration, 20 ns of MD  
455 simulation were run at constant temperature (300 K) and pressure (1 atm). Short and long-range  
456 forces were calculated every one and two time steps, respectively (each time step = 2.0 fs),  
457 constraining the covalent bonds involving hydrogen atoms to their equilibrium values. Long-  
458 range electrostatic interactions were accounted for by means of the particle mesh Ewald  
459 approach applying periodic boundary conditions. The root mean square deviation (RMSD) as a

460 function of time with respect to the starting structure for the  $\alpha$ -C atoms was computed using  
461 CPPTRAJ (63). The 3D coordinates of the structures for BcnA and BcnB subjected to the  
462 equilibration protocol described above were used for docking purposes. The two models were  
463 prepared for docking calculations by adding Kollman charges (64) with the help of  
464 AutoDockTools.

465 3D coordinates of norfloxacin, PmB, ceftazidime, gentamicin, Nile Red and  $\alpha$ -tocopherol  
466 were built in Corina (65) from the SMILES code. The 3D structure of rifampicin was extracted  
467 from the crystallographic structure PDB-ID 1LSV. The structures of the seven ligands were  
468 protonated at pH 7.0 using Epik (66) and then optimized with MMFFs force field by using  
469 MacroModel version 9.9 (<https://www.schrodinger.com/macromodel>). Additionally, the  
470 structure of polymyxin B was subjected to 100 ps of MD simulation, at 300 K. Ligands were  
471 prepared for docking calculations using AutoDockTools by adding Gasteiger charges (67) and  
472 setting all rotatable bonds free to move during the docking calculation.

473 Docking calculations of all compounds were performed by means of AutoDock 4.2.2 (68).  
474 Analysis was performed with the help of AutoDockTools. The grid point spacing was set at  
475 0.375 Å, and a hexahedral box was built with x, y, z dimensions 21.00 Å, 26.25 Å, 27.75 Å  
476 centred in the binding site of the protein. 200 runs using Lamarckian Genetic algorithm were  
477 performed, with a population size of 100, and 250000 energy evaluations. Side chains of residues  
478 Y85, W94 and Q41 were considered as flexible during the docking protocol.

479 **BCN consensus motif determination.** A subset of 187 curated 187 BcnA homologues from  
480 different bacterial species and families were used to obtain a consensus motif generated by the  
481 Gapped Local Alignment Motifs “GLAM2” tool (69). This motif was verified by analyzing an  
482 alignment of 1995 BCN homologues using CLUSTAL-omega and visualized using JalView. In

483 addition, upon submitting the predicted motif into the “GLAM2Scan” database (69) against *B.*  
484 *cennocepacia*, *P. aeruginosa* PAO1, *M. tuberculosis* H37Rv and *S. aureus* USA300, the correct  
485 homologues only were detected as BCNs for each of the organisms.

486 **Statistical Analyses.** Statistical analyses were conducted with GraphPad Prism 5.0. All  
487 results are shown as mean  $\pm$ SEM unless otherwise stated. Unless otherwise stated, data were  
488 assumed to follow a Gaussian distribution as determined by D'Agostino-Pearson omnibus K2  
489 normality test whenever possible and hence t-tests and ANOVA were used. Unpaired t-test was  
490 used to compare the means of two unmatched groups. Paired t-test was used to compare the  
491 means of two matched groups, assuming that the distribution of the before-after differences  
492 follows a Gaussian distribution. One-way ANOVA followed by Dunn's multiple comparison test  
493 was used to compare the means of three or more unmatched groups. The variances were not  
494 significantly different among the groups being statistically compared as determined by F-test,  
495 except in the *in vivo* mice infection assay (See the “Intraperitoneal infection in mice” section).  
496 The sample size (n) was chosen using GraphPad StatMate 2.0 to ensure a minimum of 80%  
497 power to detect statistically significant effects at significance level (alpha) of 0.05, two-tailed.  
498 However, the actual power of most of the assays was  $\geq$ 90% and in many cases exceeded 99%. In  
499 case of MIC assays, the experiments were repeated 3 independent times and the experiment  
500 showing the lowest fold change (if applicable) was reported.

501

## 502 **SUPPLEMENTAL MATERIAL**

503 Supplemental Results

504 Table S1. X-ray crystallography data collection and refinement statistics

505 Table S2. Strains and Plasmids

506 Figure S1. Chemical structures of antibiotics and chemicals used in this study.  
507 Figure S2. Expression and secretion profiles of BcnA and BcnB.  
508 Figure S3. Binding Assays  
509 Figure S4. BcnA and BcnB macromolecular structures and docking binding models of antibiotics  
510 into the BcnA structure.  
511 Figure S5. Nile red binding affinity of *B. cenocepacia* BcnA site-directed mutants  
512 Figure S6. Overall MD simulation analysis of the BcnA, BcnA D82A-D93A mutant and BcnB  
513 structures.  
514 Figure S7. Effects of *B. cenocepacia* BCNs on bacterial species *in vitro* and *in vivo*.

515  
516

517 **ACKNOWLEDGMENTS.** This work was funded by grants from Cystic Fibrosis Canada, the  
518 European Commission Marie Curie Career Integration Grant (projects 618095, NONANTIRES),  
519 and The Infection & Immunity Translational Research Group, Northern Ireland HSC to M.A.V;  
520 the Spanish Ministry for Economy and Competitiveness (MINECO, Refs. CTQ2011-22724 and  
521 CTQ2014-57141-R), European Commission Marie Curie grants GLYCOPHARM FP7-PITN-  
522 GA-2012-317297, and TOLLerant H2020-MSC-ETN-642157 to S.M.S.; and grants from the  
523 Canadian Institutes of Health Research Grant MOP-49597 and Cystic Fibrosis Canada to  
524 M.E.P.M. An Ontario Graduate Scholarship supported O.M.E. We thank Luke Alderwick,  
525 Institute of Microbiology and Infection, University of Birmingham for providing *M. tuberculosis*  
526 H37Rv genomic DNA, Sameer Elsayed, London Health Science Centre, for providing clinical  
527 isolates, Martin McGavin, Department of Microbiology and Immunology, the University of



528 Western Ontario for providing the *S. aureus* USA300 strain, and Alice Dubois, Queen's  
529 University for assistance with the mouse infection experiments.

530

## 531 REFERENCES

- 532 1. **WHO**. 2014. Antimicrobial resistance: Global Report on Surveillance. World Health  
533 Organization, WHO,
- 534 2. **Li XZ, Plesiat P, Nikaido H**. 2015. The challenge of efflux-mediated antibiotic resistance in  
535 Gram-negative bacteria. *Clin Microbiol Rev* **28**:337-418.
- 536 3. **Starosta AL, Lassak J, Jung K, Wilson DN**. 2014. The bacterial translation stress response.  
537 *FEMS Microbiol Rev* **38**:1172-1201.
- 538 4. **Marrakchi M, Liu X, Andreescu S**. 2014. Oxidative stress and antibiotic resistance in  
539 bacterial pathogens: state of the art, methodologies, and future trends. *Adv Exp Med Biol*  
540 **806**:483-498.
- 541 5. **Baharoglu Z, Mazel D**. 2014. SOS, the formidable strategy of bacteria against aggressions.  
542 *FEMS Microbiol Rev* **38**:1126-1145.
- 543 6. **de la Fuente-Nunez C, Reffuveille F, Fernandez L, Hancock RE**. 2013. Bacterial biofilm  
544 development as a multicellular adaptation: antibiotic resistance and new therapeutic  
545 strategies. *Curr Opin Microbiol* **16**:580-589.
- 546 7. **Poole K**. 2012. Stress responses as determinants of antimicrobial resistance in Gram-  
547 negative bacteria. *Trends Microbiol* **20**:227-234.
- 548 8. **Levy SB, Marshall B**. 2004. Antibacterial resistance worldwide: causes, challenges and  
549 responses. *Nat Med* **10**:S122-129.
- 550 9. **Alekshun MN, Levy SB**. 2007. Molecular mechanisms of antibacterial multidrug resistance.  
551 *Cell* **128**:1037-1050.
- 552 10. **Liao YT, Kuo SC, Chiang MH, Lee YT, Sung WC, Chen YH, Chen TL, Fung CP**. 2015.  
553 *Acinetobacter baumannii* Extracellular OXA-58 Is Primarily and Selectively Released via  
554 Outer Membrane Vesicles after Sec-Dependent Periplasmic Translocation. *Antimicrob*  
555 *Agents Chemother* **59**:7346-7354.
- 556 11. **Lee J, Lee EY, Kim SH, Kim DK, Park KS, Kim KP, Kim YK, Roh TY, Gho YS**. 2013.  
557 *Staphylococcus aureus* extracellular vesicles carry biologically active  $\beta$ -lactamase.  
558 *Antimicrob Agents Chemother* **57**:2589-2595.

- 559 12. **Devos S, Stremersch S, Raemdonck K, Braeckmans K, Devreese B.** 2016. Intra- and  
560 Interspecies Effects of Outer Membrane Vesicles from *Stenotrophomonas maltophilia* on  
561 beta-Lactam Resistance. *Antimicrob Agents Chemother* **60**:2516-2518.
- 562 13. **Ciofu O, Beveridge TJ, Kadurugamuwa J, Walther-Rasmussen J, Høiby N.** 2000.  
563 Chromosomal  $\beta$ -lactamase is packaged into membrane vesicles and secreted from  
564 *Pseudomonas aeruginosa*. *J Antimicrob Chemother* **45**:9-13.
- 565 14. **Loutet SA, Valvano MA.** 2010. A decade of *Burkholderia cenocepacia* virulence  
566 determinant research. *Infect Immun* **78**:4088-4100.
- 567 15. **Rhodes KA, Schweizer HP.** 2016. Antibiotic resistance in *Burkholderia* species. *Drug*  
568 *Resist Updat* **28**:82-90.
- 569 16. **El-Halfawy OM, Valvano MA.** 2013. Chemical communication of antibiotic resistance by a  
570 highly resistant subpopulation of bacterial cells. *PLoS One* **8**:e68874.
- 571 17. **Bishop RE.** 2000. The bacterial lipocalins. *Biochim Biophys Acta* **1482**:73-83.
- 572 18. **Donnarumma D, Golfieri G, Brier S, Castagnini M, Veggi D, Bottomley MJ, Delany I,**  
573 **Norais N.** 2015. *Neisseria meningitidis* GNA1030 is a ubiquinone-8 binding protein. *FASEB J*  
574 **29**:2260-2267.
- 575 19. **Handa N, Terada T, Doi-Katayama Y, Hirota H, Tame JR, Park SY, Kuramitsu S,**  
576 **Shirouzu M, Yokoyama S.** 2005. Crystal structure of a novel polyisoprenoid-binding  
577 protein from *Thermus thermophilus* HB8. *Protein Sci* **14**:1004-1010.
- 578 20. **Sisinni L, Cendron L, Favaro G, Zanotti G.** 2010. *Helicobacter pylori* acidic stress  
579 response factor HP1286 is a YceI homolog with new binding specificity. *FEBS J* **277**:1896-  
580 1905.
- 581 21. **Benndorf D, Davidson I, Babel W.** 2004. Regulation of catabolic enzymes during long-term  
582 exposure of *Delftia acidovorans* MC1 to chlorophenoxy herbicides. *Microbiology* **150**:1005-  
583 1014.
- 584 22. **Azad MA, Huang JX, Cooper MA, Roberts KD, Thompson PE, Nation RL, Li J,**  
585 **Velkov T.** 2012. Structure-activity relationships for the binding of polymyxins with human  
586  $\alpha$ -1-acid glycoprotein. *Biochem Pharmacol* **84**:278-291.
- 587 23. **Sahalan AZ, Dixon RA.** 2008. Role of the cell envelope in the antibacterial activities of  
588 polymyxin B and polymyxin B nonapeptide against *Escherichia coli*. *Int J Antimicrob*  
589 *Agents* **31**:224-227.
- 590 24. **Holm L, Rosenström P.** 2010. Dali server: conservation mapping in 3D. *Nucleic Acids Res*  
591 **38**:W545-549.
- 592 25. **Krissinel E, Henrick K.** 2007. Inference of macromolecular assemblies from crystalline  
593 state. *J Mol Biol* **372**:774-797.

- 594 26. **Camper N, Glasgow AM, Osbourn M, Quinn DJ, Small DM, McLean DT, Lundy FT,**  
595 **Elborn JS, McNally P, Ingram RJ, Weldon S, Taggart CC.** 2016. A secretory leukocyte  
596 protease inhibitor variant with improved activity against lung infection. *Mucosal Immunol*  
597 **9:669-676.**
- 598 27. **Mak P, Zdybicka-Barabas A, Cytrynska M.** 2010. A different repertoire of *Galleria*  
599 *mellonella* antimicrobial peptides in larvae challenged with bacteria and fungi. *Dev Comp*  
600 *Immunol* **34:1129-1136.**
- 601 28. **Insua JL, Llobet E, Moranta D, Perez-Gutierrez C, Tomas A, Garmendia J,**  
602 **Bengoechea JA.** 2013. Modeling *Klebsiella pneumoniae* pathogenesis by infection of the  
603 wax moth *Galleria mellonella*. *Infect Immun* **81:3552-3565.**
- 604 29. **Flower DR, North AC, Sansom CE.** 2000. The lipocalin protein family: structural and  
605 sequence overview. *Biochim Biophys Acta* **1482:9-24.**
- 606 30. **Ganfornina MD, Gutierrez G, Bastiani M, Sanchez D.** 2000. A phylogenetic analysis of  
607 the lipocalin protein family. *Mol Biol Evol* **17:114-126.**
- 608 31. **van Opijnen T, Dedrick S, Bento J.** 2016. Strain Dependent Genetic Networks for  
609 Antibiotic-Sensitivity in a Bacterial Pathogen with a Large Pan-Genome. *PLoS Pathog*  
610 **12:e1005869.**
- 611 32. **Mo CY, Manning SA, Roggiani M, Culyba MJ, Samuels AN, Sniegowski PD, Goulian**  
612 **M, Kohli RM.** 2016. Systematically Altering Bacterial SOS Activity under Stress Reveals  
613 Therapeutic Strategies for Potentiating Antibiotics. *mSphere* **1.**
- 614 33. **Sun K, Yajjala VK, Bauer C, Talmon GA, Fischer KJ, Kielian T, Metzger DW.** 2016.  
615 Nox2-derived oxidative stress results in inefficacy of antibiotics against post-influenza *S.*  
616 *aureus* pneumonia. *J Exp Med* **213:1851-1864.**
- 617 34. **Guest RL, Raivio TL.** 2016. Role of the Gram-Negative Envelope Stress Response in the  
618 Presence of Antimicrobial Agents. *Trends Microbiol* **24:377-390.**
- 619 35. **Poole K.** 2012. Bacterial stress responses as determinants of antimicrobial resistance. *J*  
620 *Antimicrob Chemother* **67:2069-2089.**
- 621 36. **El-Halfawy OM, Valvano MA.** 2014. Putrescine reduces antibiotic-induced oxidative stress  
622 as a mechanism of modulation of antibiotic resistance in *Burkholderia cenocepacia*.  
623 *Antimicrob Agents Chemother* **58:4162-4171.**
- 624 37. **Smirnova GV, Tyulenev AV, Muzyka NG, Peters MA, Oktyabrsky ON.** 2016.  
625 Ciprofloxacin provokes SOS-dependent changes in respiration and membrane potential and  
626 causes alterations in the redox status of *Escherichia coli*. *Res Microbiol*  
627 doi:10.1016/j.resmic.2016.07.008.

- 628 38. **Van Acker H, Gielis J, Acke M, Cools F, Cos P, Coenye T.** 2016. The Role of Reactive  
629 Oxygen Species in Antibiotic-Induced Cell Death in *Burkholderia cepacia* Complex  
630 Bacteria. PLoS One **11**:e0159837.
- 631 39. **Händel N, Hoeksema M, Freijo Mata M, Brul S, ter Kuile BH.** 2016. Effects of Stress,  
632 Reactive Oxygen Species, and the SOS Response on De Novo Acquisition of Antibiotic  
633 Resistance in *Escherichia coli*. Antimicrob Agents Chemother **60**:1319-1327.
- 634 40. **Dwyer DJ, Collins JJ, Walker GC.** 2015. Unraveling the physiological complexities of  
635 antibiotic lethality. Annu Rev Pharmacol Toxicol **55**:313-332.
- 636 41. **Boca S, Koestler F, Ksas B, Chevalier A, Leymarie J, Fekete A, Mueller MJ, Havaux**  
637 **M.** 2014. *Arabidopsis* lipocalins AtCHL and AtTIL have distinct but overlapping functions  
638 essential for lipid protection and seed longevity. Plant Cell Environ **37**:368-381.
- 639 42. **Macedo-Marquez A, Vazquez-Acevedo M, Ongay-Larios L, Miranda-Astudillo H,**  
640 **Hernandez-Munoz R, Gonzalez-Halphen D, Grolli S, Ramoni R.** 2014. Overexpression  
641 of a monomeric form of the bovine odorant-binding protein protects *Escherichia coli* from  
642 chemical-induced oxidative stress. Free Radic Res **48**:814-822.
- 643 43. **Hare NJ, Scott NE, Shin EH, Connolly AM, Larsen MR, Palmisano G, Cordwell SJ.**  
644 2011. Proteomics of the oxidative stress response induced by hydrogen peroxide and  
645 paraquat reveals a novel AhpC-like protein in *Pseudomonas aeruginosa*. Proteomics  
646 **11**:3056-3069.
- 647 44. **Søballe B, Poole RK.** 1999. Microbial ubiquinones: multiple roles in respiration, gene  
648 regulation and oxidative stress management. Microbiology **145 ( Pt 8)**:1817-1830.
- 649 45. **Nowicka B, Kruk J.** 2010. Occurrence, biosynthesis and function of isoprenoid quinones.  
650 Biochim Biophys Acta **1797**:1587-1605.
- 651 46. **Sambrook J, Fritsch EF, Maniatis T.** 1990. Molecular cloning: a laboratory manual, 2nd  
652 ed. Cold Spring Harbor Laboratory, Cold Spring Harbor, New York.
- 653 47. **Cohen SN, Chang AC, Hsu L.** 1972. Nonchromosomal antibiotic resistance in bacteria:  
654 genetic transformation of *Escherichia coli* by R-factor DNA. Proc Natl Acad Sci U S A  
655 **69**:2110-2114.
- 656 48. **Craig FF, Coote JG, Parton R, Freer JH, Gilmour NJ.** 1989. A plasmid which can be  
657 transferred between *Escherichia coli* and *Pasteurella haemolytica* by electroporation and  
658 conjugation. J Gen Microbiol **135**:2885-2890.
- 659 49. **Figurski DH, Helinski DR.** 1979. Replication of an origin-containing derivative of plasmid  
660 RK2 dependent on a plasmid function provided in *trans*. Proc Natl Acad Sci USA **76**:1648-  
661 1652.

- 662 50. **Rosales-Reyes R, Aubert DF, Tolman JS, Amer AO, Valvano MA.** 2012. *Burkholderia*  
663 *cenoepecia* type VI secretion system mediates escape of type II secreted proteins into the  
664 cytoplasm of infected macrophages. PLoS ONE 7:e41726.
- 665 51. **CLSI.** 2012. Methods for Dilution Antimicrobial Susceptibility Tests for Bacteria That Grow  
666 Aerobically;  
667 Approved Standard—Ninth Edition. CLSI document M07-A9. Clinical and Laboratory  
668 Standards Institute, Wayne, PA.
- 669 52. **Harding CR, Schroeder GN, Collins JW, Frankel G.** 2013. Use of *Galleria mellonella* as  
670 a model organism to study *Legionella pneumophila* infection. J Vis Exp  
671 doi:10.3791/50964:e50964.
- 672 53. **Grochulski P, Fodje MN, Gorin J, Labiuk SL, Berg R.** 2011. Beamline 08ID-1, the prime  
673 beamline of the Canadian Macromolecular Crystallography Facility. J Synchrotron Radiat  
674 18:681-684.
- 675 54. **Battye TG, Kontogiannis L, Johnson O, Powell HR, Leslie AG.** 2011. iMOSFLM: a new  
676 graphical interface for diffraction-image processing with MOSFLM. Acta Crystallogr D Biol  
677 Crystallogr 67:271-281.
- 678 55. **Winn MD, Ballard CC, Cowtan KD, Dodson EJ, Emsley P, Evans PR, Keegan RM,  
679 Krissinel EB, Leslie AG, McCoy A, McNicholas SJ, Murshudov GN, Pannu NS,  
680 Potterton EA, Powell HR, Read RJ, Vagin A, Wilson KS.** 2011. Overview of the CCP4  
681 suite and current developments. Acta Crystallogr D Biol Crystallogr 67:235-242.
- 682 56. **Bunkoczi G, Echols N, McCoy AJ, Oeffner RD, Adams PD, Read RJ.** 2013.  
683 Phaser.MRage: automated molecular replacement. Acta Crystallogr D Biol Crystallogr  
684 69:2276-2286.
- 685 57. **Terwilliger TC, Grosse-Kunstleve RW, Afonine PV, Moriarty NW, Zwart PH, Hung  
686 LW, Read RJ, Adams PD.** 2008. Iterative model building, structure refinement and density  
687 modification with the PHENIX AutoBuild wizard. Acta Crystallogr D Biol Crystallogr  
688 64:61-69.
- 689 58. **Emsley P, Lohkamp B, Scott WG, Cowtan K.** 2010. Features and development of Coot.  
690 Acta Crystallogr D Biol Crystallogr 66:486-501.
- 691 59. **Afonine PV, Grosse-Kunstleve RW, Echols N, Headd JJ, Moriarty NW, Mustyakimov  
692 M, Terwilliger TC, Urzhumtsev A, Zwart PH, Adams PD.** 2012. Towards automated  
693 crystallographic structure refinement with phenix.refine. Acta Crystallogr D Biol Crystallogr  
694 68:352-367.
- 695 60. **Murshudov GN, Skubak P, Lebedev AA, Pannu NS, Steiner RA, Nicholls RA, Winn  
696 MD, Long F, Vagin AA.** 2011. REFMAC5 for the refinement of macromolecular crystal  
697 structures. Acta Crystallogr D Biol Crystallogr 67:355-367.

- 698 61. **Kobylarz MJ, Grigg JC, Takayama SJ, Rai DK, Heinrichs DE, Murphy ME.** 2014.  
699 Synthesis of L-2,3-diaminopropionic acid, a siderophore and antibiotic precursor. *Chem Biol*  
700 **21**:379-388.
- 701 62. **Wang J, Kollman PA.** 2001. Automatic parameterization of force field by systematic search  
702 and genetic algorithms. *J Com Chem* **22**:1219-1228.
- 703 63. **Roe DR, Cheatham III TE.** 2013. PTRAJ and CPPTRAJ: Software for Processing and  
704 Analysis of Molecular Dynamics Trajectory Data. *J Chem Theory Comput* **9**:3084–3095.
- 705 64. **Besler BH, Merz KM, Kollman PA.** 1990. Atomic Charges Derived from Semiempirical  
706 Methods. *J Comp Chem* **11**:431-439.
- 707 65. **Sadowski J, Gasteiger J, Klebe G.** 1994. Comparison of Automatic Three-Dimensional  
708 Model Builders Using 639 X-ray Structures. *J Chem Inf Comput Sci* **34**:1000–1008.
- 709 66. **Greenwood JR, Calkins D, Sullivan AP, Shelley JC.** 2010. Towards the comprehensive,  
710 rapid, and accurate prediction of the favorable tautomeric states of drug-like molecules in  
711 aqueous solution. *J Comput Aided Mol Des* **24**:591-604.
- 712 67. **Gasteiger J, Marsili M.** 1980. Iterative partial equalization of orbital electronegativity-a  
713 rapid access to atomic charges. *Tetrahedron* **36**:3219-3228.
- 714 68. **Morris GM, Huey R, Lindstrom W, Sanner MF, Belew RK, Goodsell DS, Olson AJ.**  
715 2009. AutoDock4 and AutoDockTools4: Automated docking with selective receptor  
716 flexibility. *J Comput Chem* **30**:2785-2791.
- 717 69. **Frith MC, Saunders NF, Kobe B, Bailey TL.** 2008. Discovering sequence motifs with  
718 arbitrary insertions and deletions. *PLoS Comput Biol* **4**:e1000071.
- 719 70. **Zuker M.** 2003. Mfold web server for nucleic acid folding and hybridization prediction.  
720 *Nucleic Acids Res* **31**:3406-3415.
- 721
- 722

723 **Figure Legends**

724

725 FIG. 1. *B. cenocepacia* BcnA confers resistance to hydrophobic but not hydrophilic antibiotics.

726 (A) MIC by broth microdilution of different antibiotics in cation-adjusted MHB at 18-24 h

727 (representative from 3 independent experiments). (B) Luciferase expression assay of the *B.*

728 *cenocepacia* BcnA (OME61) in response to antibiotics at 3 h. n= 6 from 2 different clones.

729 Results are shown as percentage of relative light units RLU/OD<sub>600</sub> relative to the control

730 (untreated K56-2 background). The %OD<sub>600</sub> are shown in Fig. S2D. The mean RLU/OD<sub>600</sub> of the

731 control is 1.3464. \* p<0.05 and \*\*\* p<0.001 from unpaired two-sided Student's t-tests compared

732 to the respective control conditions. (C) Genomic organization of the *B. cenocepacia* K56 region.

733 The asterisk denotes that the transcribed intergenic sequence between *bcnA* and *bcnB* has the

734 potential to form strong secondary structures as determined with mFold

735 (<http://unafold.rna.albany.edu/?q=mfold/download-mfold>) (70).

736

737 FIG. 2. BCNs from different bacteria can restore full antibiotic resistance in *B. cenocepacia*

738  $\Delta bcnA$ . (A) cfu count on LB agar containing PmB, from 3 independent experiments, n=6,

739 asterisks denote difference from  $\Delta bcnA$  pSCRhaB2 mutant. \* p<0.05, \*\* p<0.01 and \*\*\*

740 p<0.001 determined by unpaired two-sided Student's t-tests. (B) MIC by Etest against rifampicin

741 (Rif), ceftazidime (Cef) and ciprofloxacin (Cipro), a representative of 3 independent

742 experiments. The highest rifampicin concentration on the Etest strips is 32  $\mu\text{g/ml}$ ;  $\geq 64$  indicates

743 that an MIC could not be detected within the Etest concentration range and would be equal to 64

744  $\mu\text{g/ml}$  or higher.

745

746 FIG. 3. BCNs bind antibiotics and other molecules hydrophobic in nature with high affinity. (A)  
747 Antibiotic assay showing reduction in concentration of hydrophobic antibiotics due to  
748 sequestration by BcnA, n=3 from three independent experiments. (B) *in vitro* binding assay  
749 showing binding inhibition constant ( $K_i$ ) of antibiotics against 1.5  $\mu$ M Nile Red binding to 1.5  
750  $\mu$ M BcnA in PBS, 3 independent experiments, n=5.

751  
752 FIG. 4. Structural analysis of BcnA and BcnB and ligand docking modeling. (A) BcnA (blue) is  
753 a monomer. (B) BcnB (protomer 1, chain C, peach; protomer 2, chain D, grey) is a dimer. (C)  
754 Superposition of BcnA and BcnB with dissimilar tunnel opening loops boxed. (D) Docked  
755 structure of PmB in complex with the BcnA crystallographic structure. (E) Docking model  
756 presenting the superimposition of the two best predicted binding modes of Nile Red (magenta  
757 and cyan) and  $\alpha$ -tocopherol (yellow) when docked into the BcnA crystallographic structure.

758  
759 FIG. 5. *B. cenocepacia* BcnA protects *P. aeruginosa* *in vitro* and *in vivo*. (A) *in vitro* protection  
760 of *P. aeruginosa* PAO1 against PmB with 1.5  $\mu$ M of BcnA or BcnB, n=8 from 4 independent  
761 experiments. (B) Protection of *P. aeruginosa* Q502 from PmB killing in an intraperitoneal  
762 infection of C57BL/6 mice, significant difference determined by Kruskal-Wallis test. (C) The  
763 survival of *G. mellonella* larvae infected with *P. aeruginosa* PAO1 compared to control group  
764 injected with sterile PBS; 10 larvae/group; the results are obtained from 3 independent  
765 experiments. The survival of both PAO1 and PAO1-BcnB treated larvae is significantly different  
766 from that of PAO1-BcnA treated group at p= 0.0165 and 0.0303 respectively. (D) PAO1 cfu/ml  
767 recovered from larval hemolymph 200 min post-infection; n=10 from 2 independent



768 experiments. \*  $p < 0.05$ , \*\*  $p < 0.01$  and \*\*\*  $p < 0.001$  from unpaired two-sided Student's t-tests  
769 compared to the respective control conditions.

770

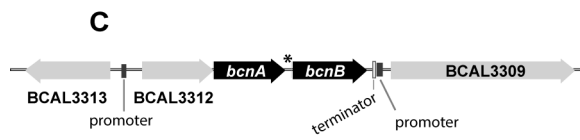
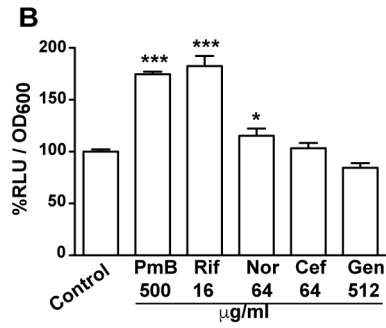
771 FIG. 6. Fat-soluble vitamins inhibit BCN-mediated antibiotic binding. (A) The survival of *G.*  
772 *mellonella* larvae at 20 h post-infection in an *in vivo* protection assay of *P. aeruginosa* PAO1 by  
773 1.5  $\mu\text{M}$  BcnA in the presence or absence of 10  $\mu\text{M}$   $\alpha$ -tocopherol (vitamin E) or menaquinone  
774 (vitamin K2), 10 larvae per group; the results are obtained from 4 independent experiments. \*  
775  $p < 0.05$ , \*\*  $p < 0.01$  and \*\*\*  $p < 0.001$  from unpaired two-sided Student's t-tests. (B) Model of the  
776 mechanism of resistance by BcnA (top) and its inhibition by the fat-soluble vitamins (bottom).

777

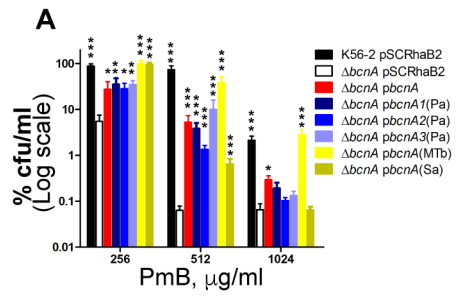
778

**A**

	MIC ( $\mu\text{g/ml}$ )		
	K56-2	$\Delta\text{bcnA}$	$\Delta\text{bcnB}$
PmB	$\geq 4096$	2048	$\geq 4096$
Rifampicin	256	64	256
Norfloxacin	128	32	128
Ceftazidime	32	8	32
Meropenem	1	0.5	1
Gentamicin	2048	2048	2048
Minocycline	2	0.5	2
Trimethoprim	8	4	8
Azithromycin	64	64	64

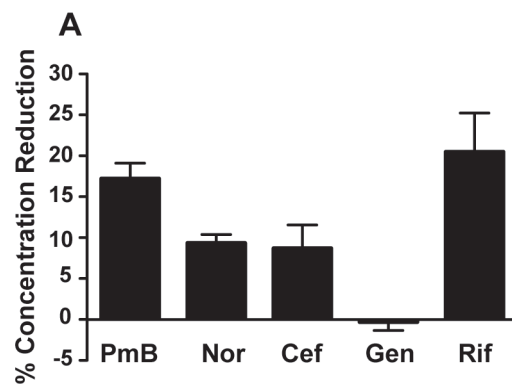


***Bcn* region in K56-2/J2315**  
4555 bp



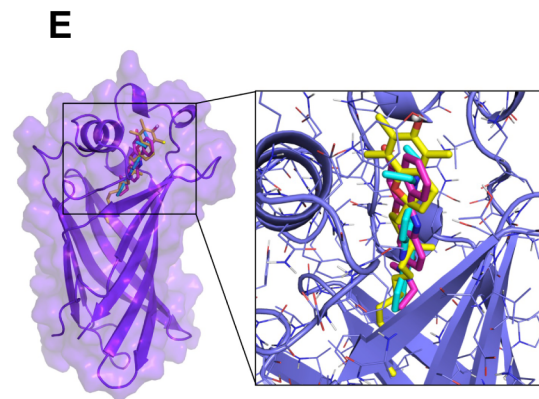
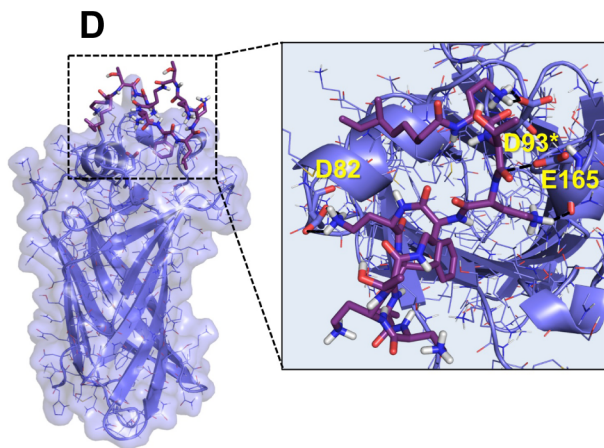
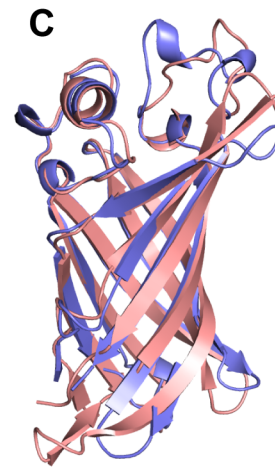
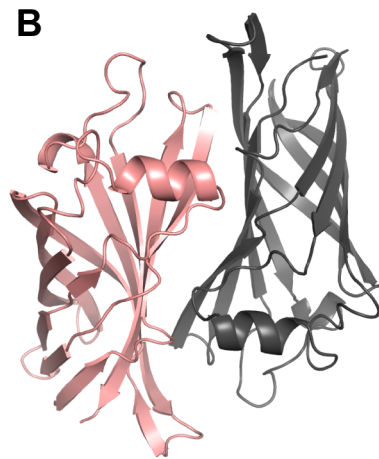
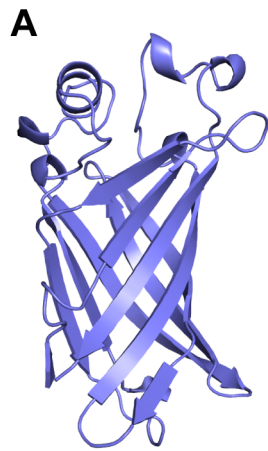
**B**

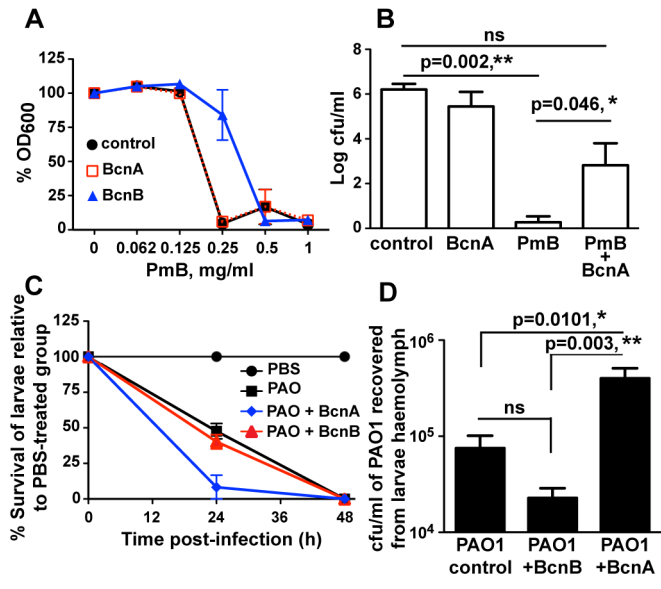
	MIC by Etest, $\mu\text{g/ml}$		
	Rif	Cef	Cipro
K56-2 pSCRhaB2	$\geq 64$	8	4
$\Delta bcnA$ pSCRhaB2	16	2	2
$\Delta bcnA$ pbcnA	$\geq 64$	8	4
$\Delta bcnA$ pbcnA1 (Pa)	$\geq 64$	8	4
$\Delta bcnA$ pbcnA2 (Pa)	32	8	4
$\Delta bcnA$ pbcnA3 (Pa)	$\geq 64$	8	4
$\Delta bcnA$ pbcnA (MTb)	$\geq 64$	8	4
$\Delta bcnA$ pbcnA (Sa)	$\geq 64$	8	4

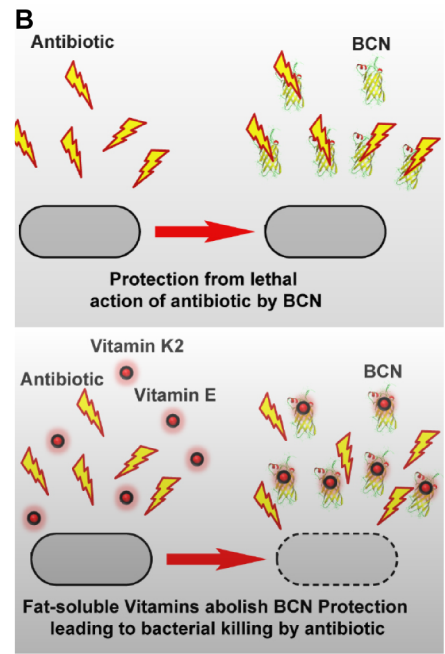
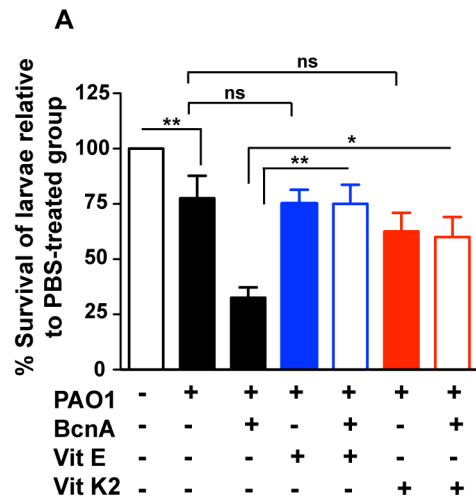


**B**

	$K_i$ , mM	SE	$r^2$
PmB	0.67	0.15	0.96
PmBN	5.08	2.54	0.35
Rif	$1.65 \cdot 10^{-2}$	$2.6 \cdot 10^{-3}$	0.97
Nor	0.40	0.29	0.86
Cef	16.9	8.45	0.33
Gen	115.4	57.7	0.005
Vit E	$4.17 \cdot 10^{-4}$	$2.04 \cdot 10^{-4}$	0.98
Vit K2	$5.69 \cdot 10^{-4}$	$2.8 \cdot 10^{-4}$	0.94







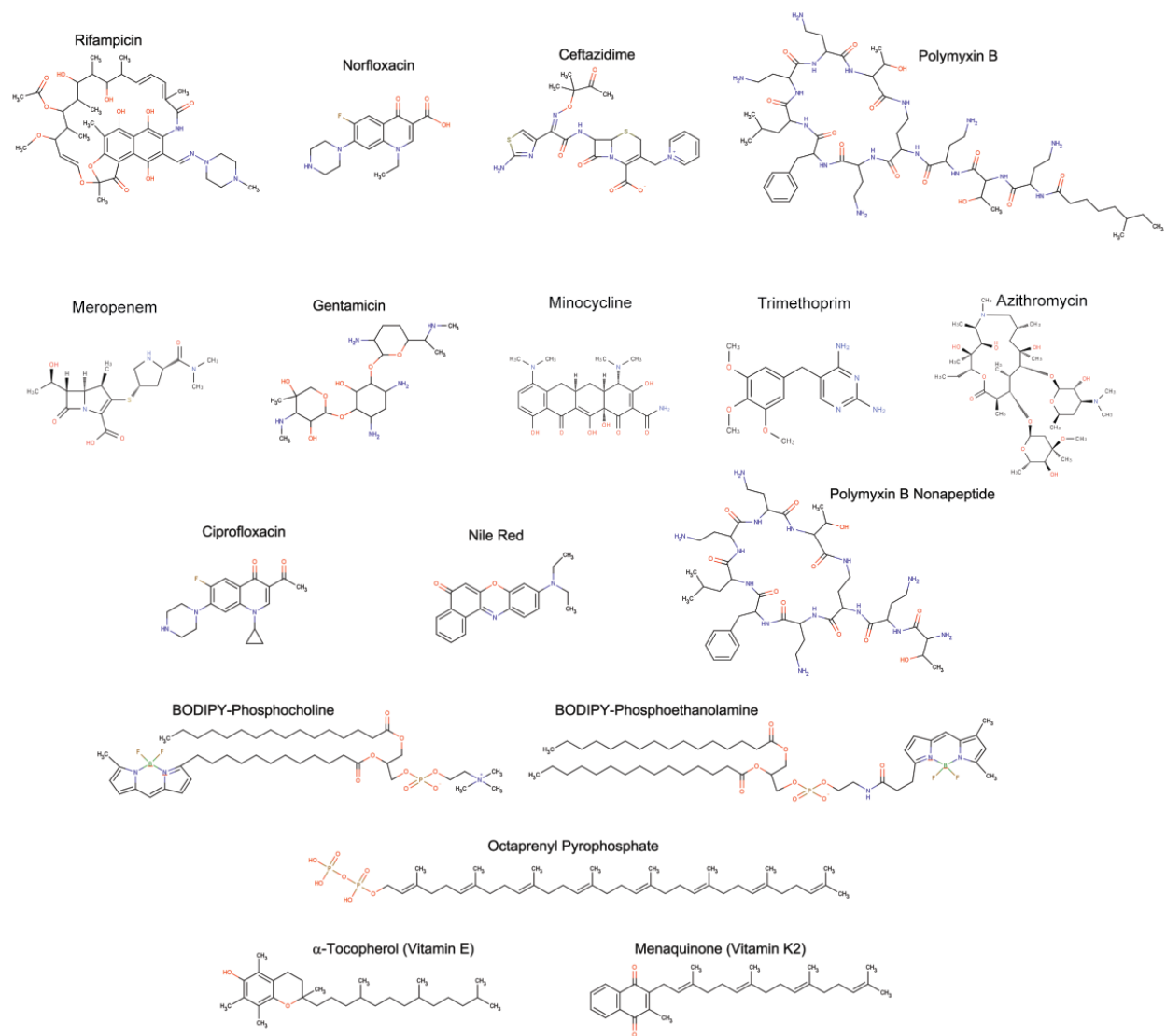


**Fig. S1.** Chemical structures of antibiotics and chemicals used in this study.



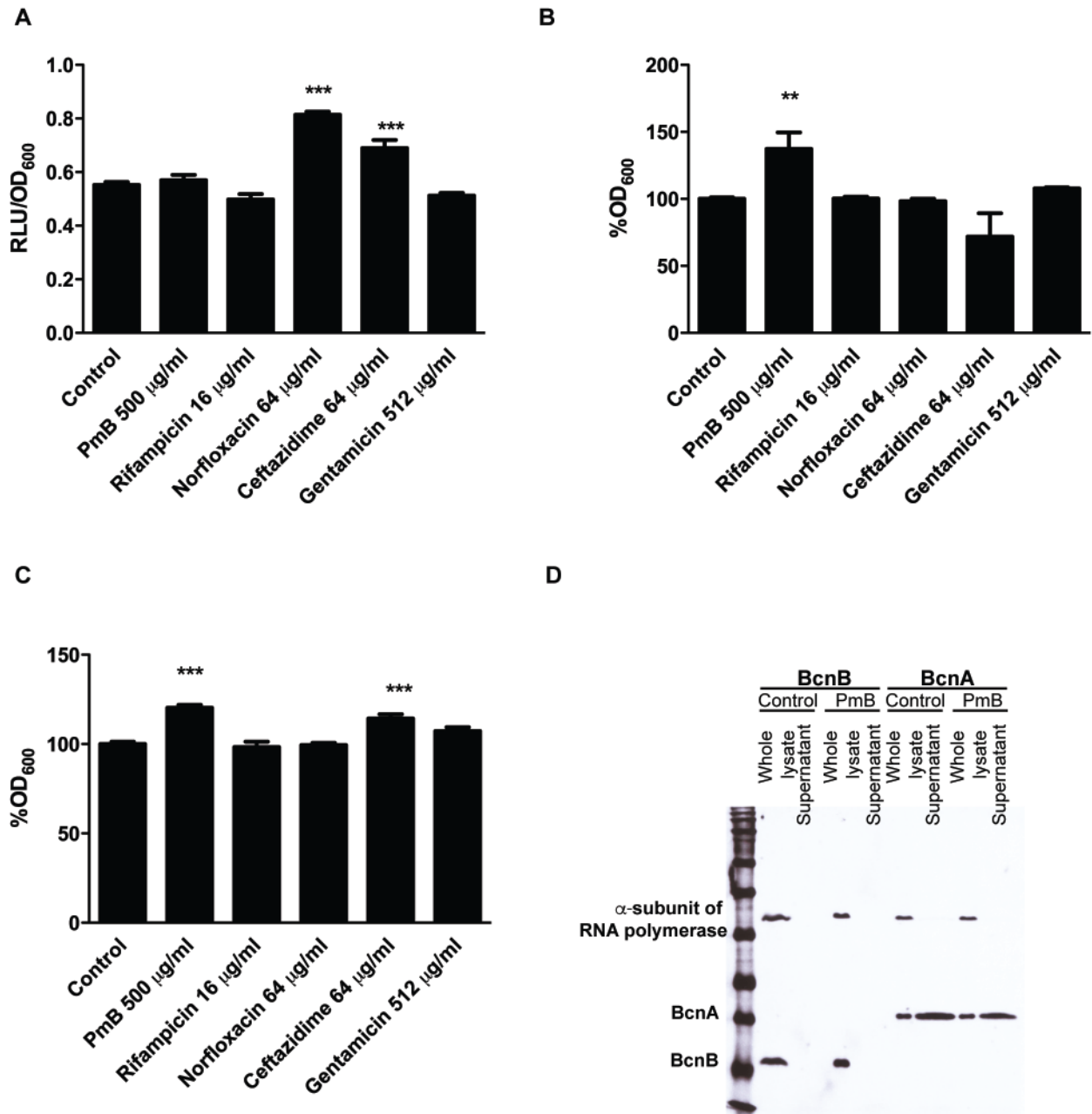


**Fig. S2. Expression and secretion profiles of BcnA and BcnB.** (A) Luciferase expression assay of BcnB and the relative growth of cells in the luminescence expression assay of the different *B. cenocepacia* BCNs in response to antibiotics at 3 h. Expression of BcnB (OME60). n=6 from 2 different clones. Results are shown as mean of relative light units RLU/OD<sub>600</sub>  $\pm$ SEM. (B) Growth in the expression assay of BcnB (OME60). n=6 from 2 different clones. The mean OD<sub>600</sub> of the control is 0.0963. (C) Growth in the expression assay of BcnA and the associated CybB (OME61) shown in Fig. 1B. n= 6 from 2 different clones. Results are shown as mean of percentage of OD<sub>600</sub> relative to the control (untreated K56-2 background)  $\pm$ SEM. The mean OD<sub>600</sub> of the control is 0.0998. \* p<0.05, \*\* p<0.01 and \*\*\* p<0.001 from one-way ANOVA tests of overall p<0.001 and Bonferroni's post-hoc test compared to the respective untreated control conditions. (D) BcnA is the only secreted *B. cenocepacia* BCN; proteins (carrying a C-terminal FLAG-tag) were detected in whole cell lysates and supernatants of control untreated cultures or cultures treated with 2  $\mu$ g/ml PmB by Western blot using anti-FLAG antibody. The  $\alpha$ -subunit of the RNA polymerase was used as a control for cell lysis. Representative of 3 independent experiments.

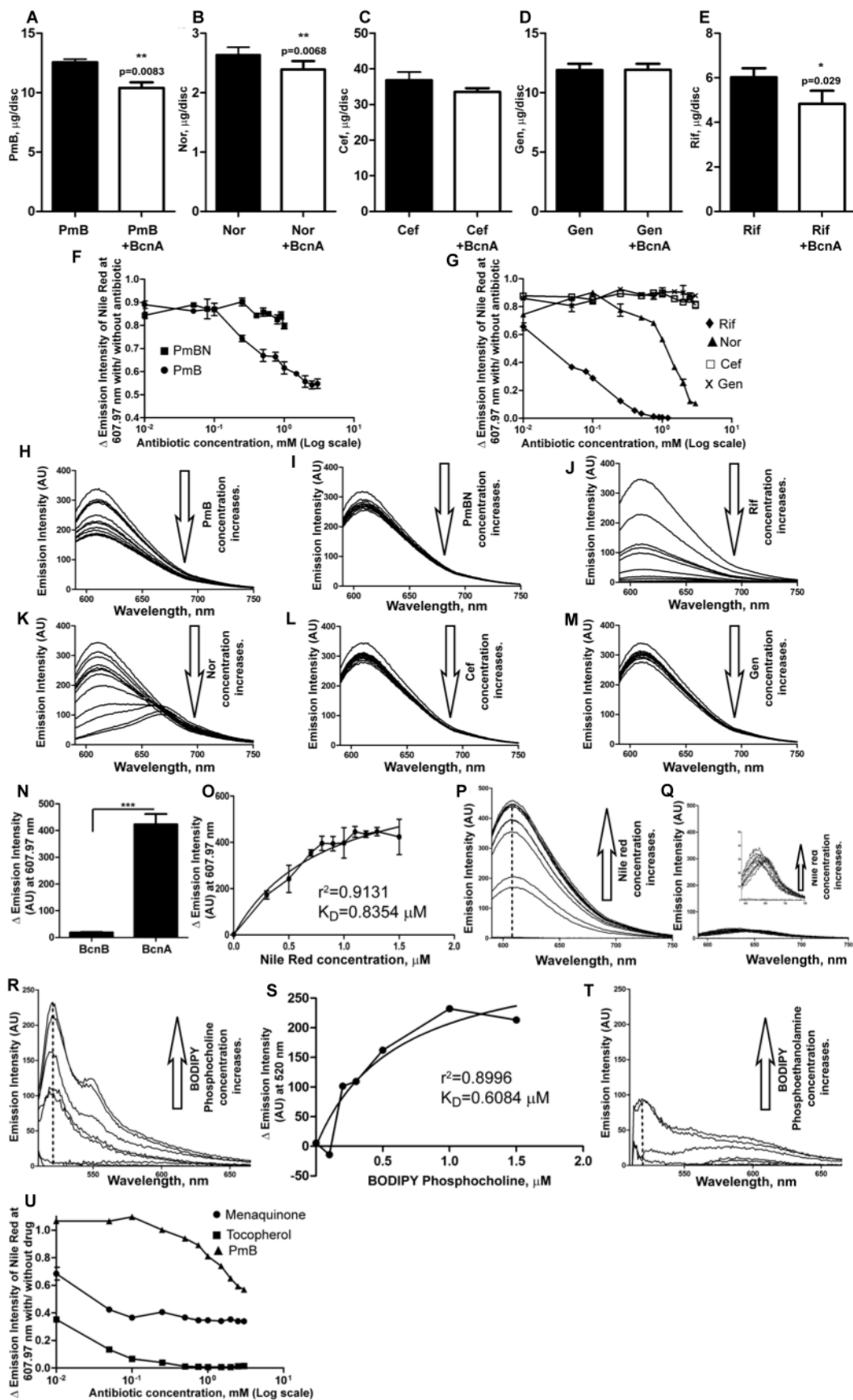


**Fig. S3. Binding Assays.** (A-E) Antibiotic bioassay results showing mean antibiotic disc contents  $\pm$ SEM following mixing with BcnA and passing through centrifugal filter units of MWCO 10 KDa compared to control antibiotic solutions. \*  $p<0.05$ ,

and \*\*  $p < 0.01$  from paired student's t-tests compared to the respective control conditions.  $n=3$  from 3 independent experiments. At this sample size, the actual power of the assay to detect statistically significant effects at significance level (alpha) of 0.05, two-tailed is  $>99\%$ . (F-G) Binding displacement assays of Nile Red from  $1.5 \mu\text{M}$  BcnA- $1.5 \mu\text{M}$  Nile Red complex by antibiotics and other chemicals. 3 independent experiments,  $n=5$ . (H-M) Binding displacement isotherms showing the displacement of Nile Red by different antibiotics from its complex with BcnA. Mean of  $n=3$  from a representative of 3 independent experiments. (N) The affinity of  $1.5 \mu\text{M}$  BcnA compared to that of  $1.5 \mu\text{M}$  BcnB to bind  $1.5 \mu\text{M}$  Nile Red,  $n=5$  from 3 independent experiments. \*\*\*  $p < 0.001$  from unpaired two-sided Student's t-test. (O) *In vitro* binding assay of  $1.5 \mu\text{M}$  BcnA to Nile Red in PBS, 3 independent experiments,  $n=5$ . (P and Q) Binding isotherms from the fluorometric assays showing the interaction between BcnA (P) or BcnB (Q) and Nile Red. Mean of  $n=3$  from a representative of 3 independent experiments. (R-T) Nile red binding affinity of BcnA to BODIPY phosphocholine (R and S) and BODIPY phosphoethanolamine (T),  $n=4$  from 2 independent experiments. (U) Binding displacement assays of Nile Red from  $1.5 \mu\text{M}$  BcnA- $1.5 \mu\text{M}$  Nile Red complex by vitamins.  $n=5$  from 3 independent experiments

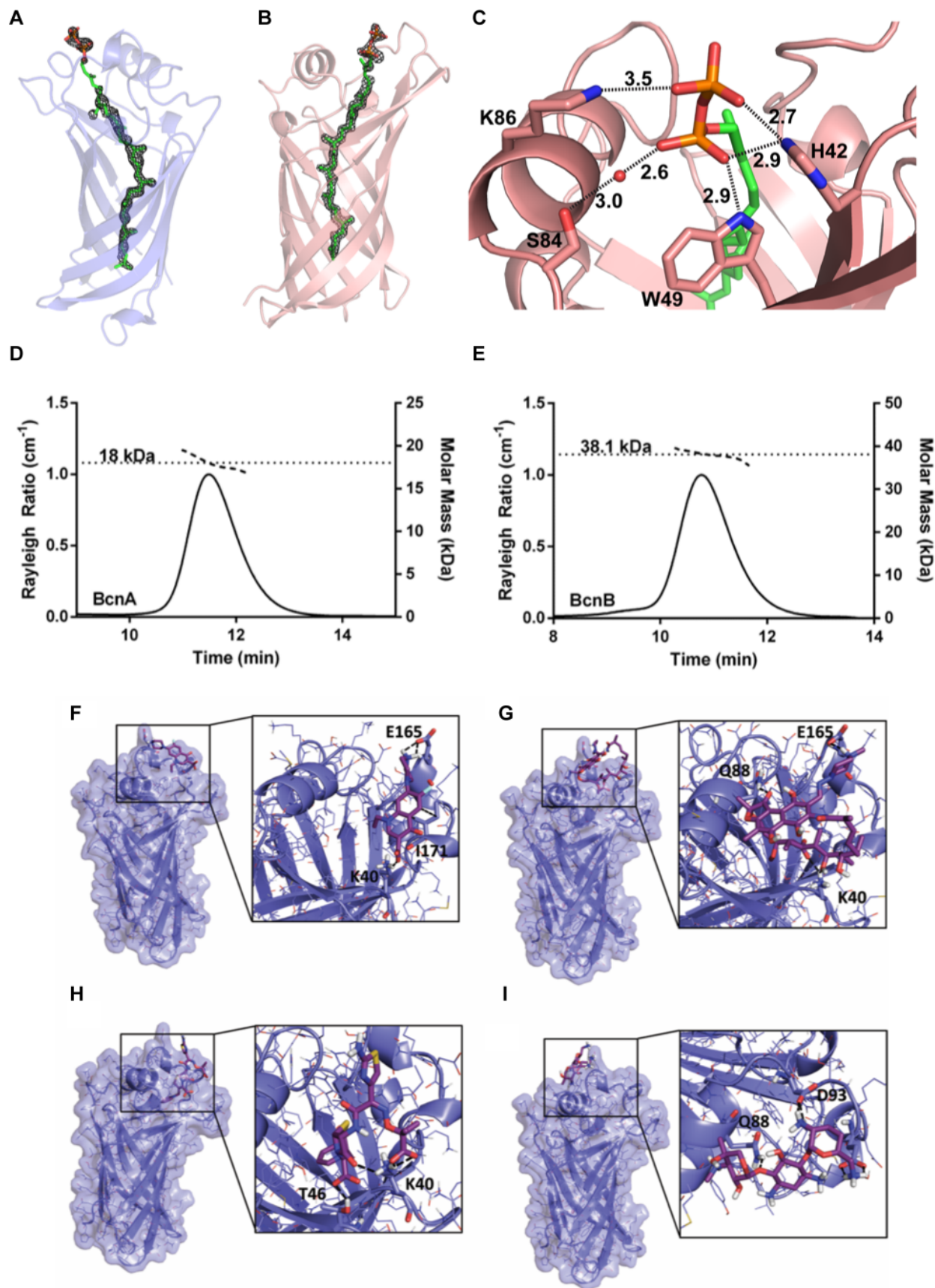


**Fig. S4. BcnA and BcnB macromolecular structures and docking binding models of antibiotics into the BcnA structure.** BcnA (A) and BcnB (B) possess electron density within the interior of the protein cavities that was modeled as octaprenyl pyrophosphate (OTP; carbon, green; phosphate, brown; oxygen, red). OTP omit maps (Fo-Fc) are contoured at

3.0  $\sigma$  and shown in black mesh. (C) The cavity opening of BcnB provides a hydrogen-bonding network to the OTP pyrophosphate via amino acids H42, W49, K86, and S84 through a water (red sphere) bridge. These residues are shown as stick figures (carbon, peach; nitrogen, blue; oxygen, red). Hydrogen bonds are represented as dotted lines with distances between the hydrogen bond donor and acceptor atoms shown in Å. The molar mass determination of BcnA (D) and BcnB (E) in solution were determined by SEC-MALS; the elution profiles (solid lines) represent the intensity of scattered light and are expressed as rayleigh ratios. The measured molar masses (dashed line) were constrained to the single elution peak for each protein. The dotted lines represent the final calculated mass for each protein. The BcnA crystallographic structure was used to perform molecular docking experiments. Selected docked binding modes of the antibiotics norfloxacin (F), rifampicin (G), ceftazidime (H), and gentamicin (I) into the BcnA structure (displayed in blue) and main residues interacting with the different ligands (CPK colors) are shown.

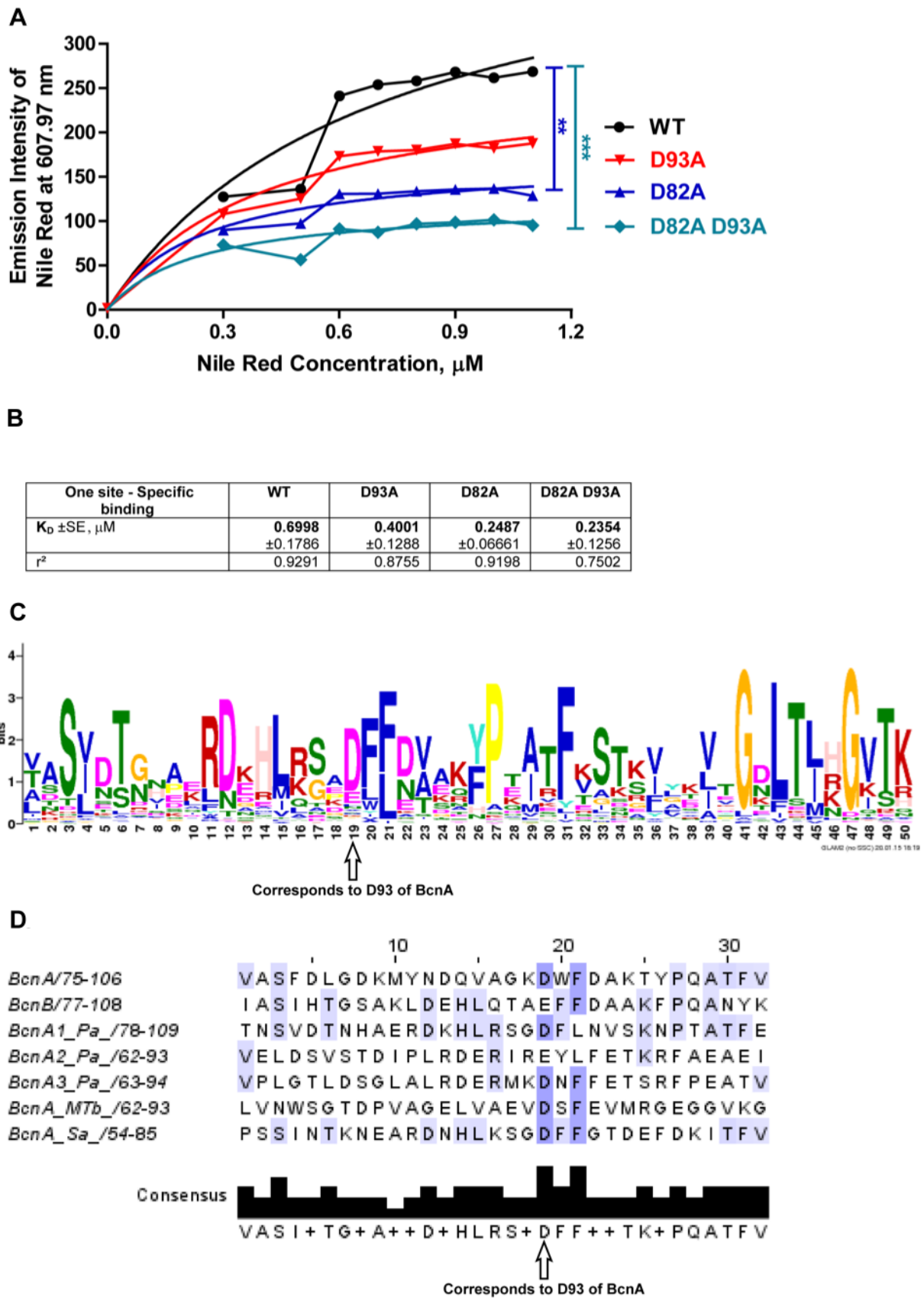


**Fig. S5.** Nile red binding affinity of *B. cenocepacia* BcnA site-directed mutants compared to the wild type, n=4, 2 independent experiments; the smooth lines show the non-linear least square regression analysis of the binding isotherms;

one-way ANOVA (with overall  $p < 0.001$ ) Dunn's Multiple Comparison Test (A-B). (C) Consensus motif of BCN family of proteins. (D) Sequence alignment and consensus motif of BCN homologues used in this study.

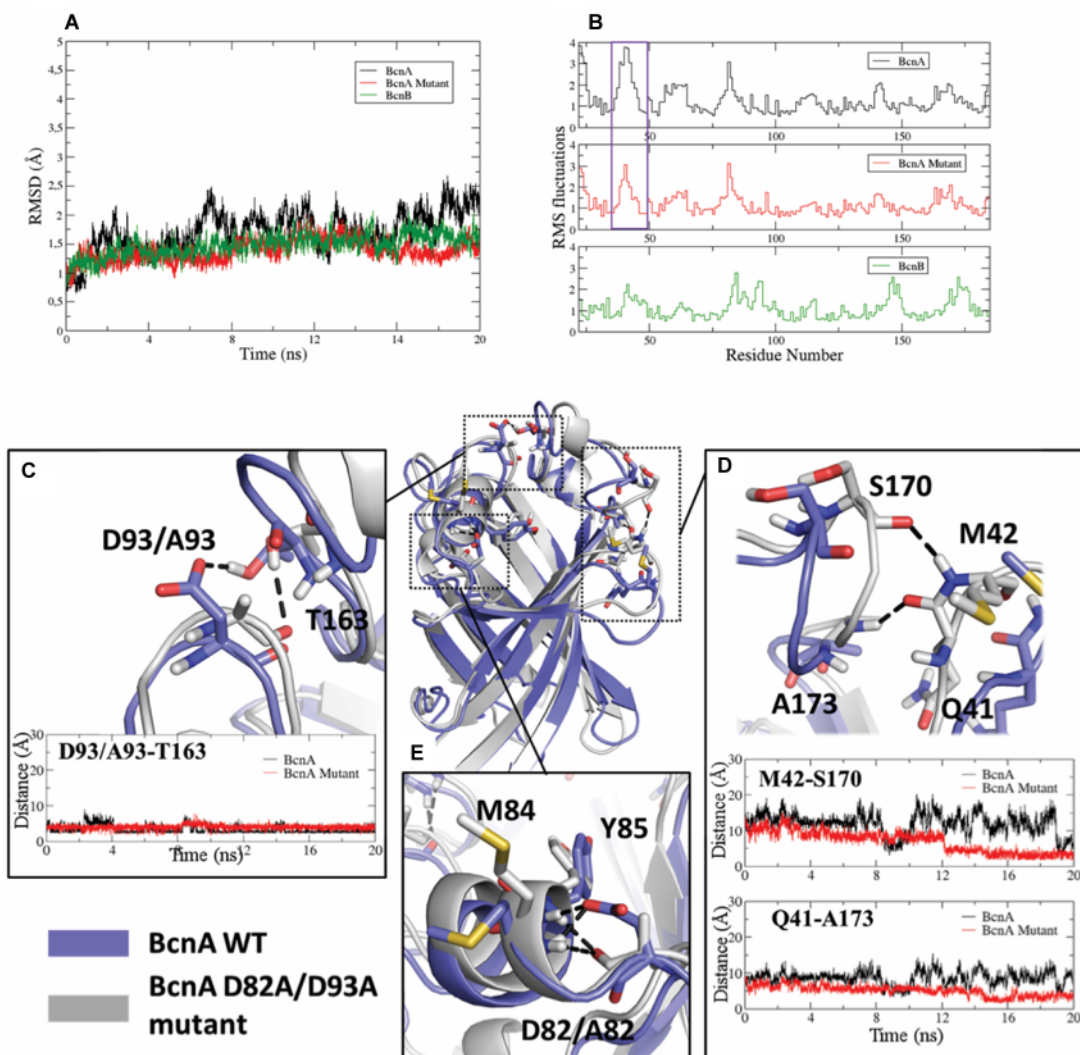
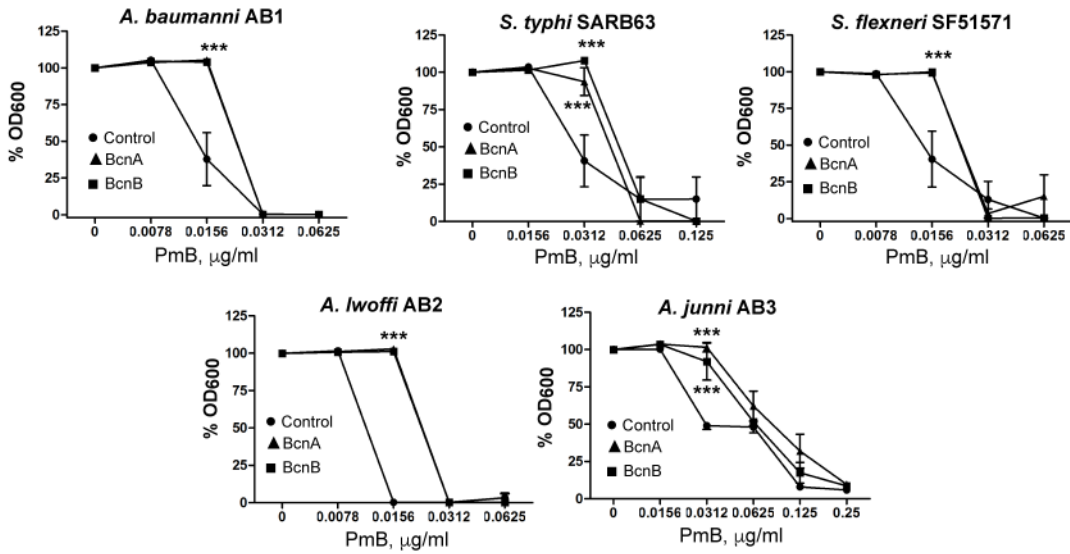


**Fig. S6. (A-B)** Overall MD simulation analysis of the BcnA, BcnA D82A-D93A mutant and BcnB structures. (A) Plot showing the RMSD of the position of the  $\alpha$ -carbons of BcnA (black), BcnA D82A-D93A mutant (red) and BcnB (green) during the 20ns MD simulation. (B) Plot showing the RMS fluctuations of the position of all atoms during the 20ns MD simulation. The V38-E47 loop marked in the purple box remarks the higher flexibility observed in the case of the BcnA WT (black) compared to the BcnA D82A-D93A mutant (in red, lower fluctuations).

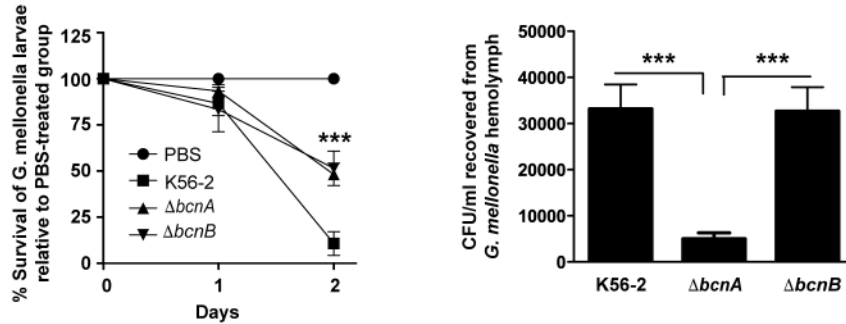
**(C-E)** Superimposition of the BcnA wild type (WT, indigo) and BcnA D82A/D93A mutant (grey) minimized average structures from the last 5ns of MD simulation. (C) Interaction between D93/A93 and T163 respectively, along with a plot representing the interaction distance between the D93 carboxylate oxygen and T163 side chain OH group in the BcnA WT, and the A93 carbonyl oxygen and T163 side chain OH group in the BcnA D82A/D93A mutant (marked with black dotted lines) along the MD simulation time. (D) Hydrogen bonds (marked with black dotted lines) between the M42 NH group and S170 CO group, and the Q41 CO group and A173 NH group (BcnA WT in indigo, and BcnA D82A/D93A mutant in grey), together with the plots of the corresponding interaction distances along the MD simulation time. (E) Detailed views of the hydrogen bonds established between the NH groups from M84 and Y85 and the D82 carboxylate oxygen in the BcnA WT, and the same NH groups from M84 and Y85 and the carbonyl oxygen from A82 in the BcnA D82A/D93A mutant (marked with black dotted lines).



**A**



**B**



**C**

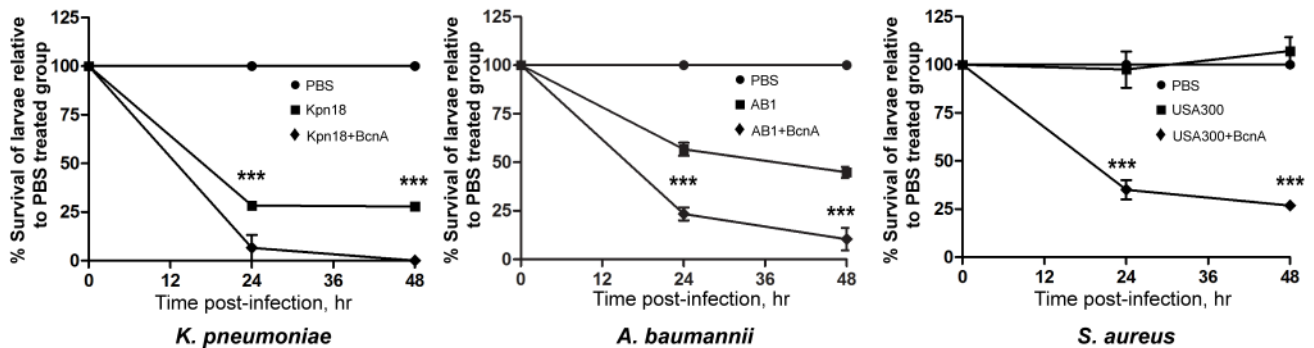


**Fig. S7. Effects of *B. cenocepacia* BCNs on bacterial species *in vitro* and *in vivo*.** (A) *in vitro* protection assays against PmB with 1.5 µM of BcnA or BcnB on *A. baumannii* AB1 (n=6 from 2 independent experiments), *Salmonella typhi* SARB63 (n=7 from 3 independent experiments), *Shigella flexneri* SF51571 (n=7 from 3 independent experiments), *Acinetobacter Iwoffii* AB2 (n=5 from 2 independent experiments), and *Acinetobacter junni* AB3 (n=5 from 2 independent experiments). Mean ±SEM. \* p<0.05, \*\* p<0.01 and \*\*\* p<0.001 determined by 2-way ANOVA (with overall p<0.001 for AB1, AB2, AB3 and SF51571, p=0.001 for SARB63) and Bonferroni post-hoc tests. (B) Survival of  $\Delta bcnA$  and  $\Delta bcnB$  in *Galleria mellonella* larvae over a 48-h infection. 10 larvae per group; the results are obtained from 3 independent experiments and shown as mean of % larval survival in each experiment ±SEM. \*\*\* p<0.001 determined by 2-way ANOVA (with overall p<0.001) and Bonferroni post-hoc tests. At the chosen sample size (n), the actual power of the assay to detect statistically significant effects at significance level (alpha) of 0.05, two-tailed is 90-95%. The right graph shows the bacterial recovery from hemolymph at 200 min postinfection; n=10 from 2 independent experiments shown as mean ±SEM. \*\*\*

p<0.001 from one-way ANOVA test (overall p<0.001) and Bonferroni's post-hoc test. At the chosen sample size (n), the actual power of the assay to detect statistically significant effects at significance level (alpha) of 0.05, two-tailed is >99%. \* p<0.05, \*\*\* p<0.001. (C) *in vivo* protection assay using *Galleria mellonella* infections. Each larva was injected with 10  $\mu$ l of suspensions of different bacteria in PBS with or without BcnA. The survival was monitored over time and compared to control group injected with sterile PBS. Each group included 10 larvae. Data are from 3 independent experiments. \* p<0.05, \*\* p<0.01 and \*\*\* p<0.001 determined by 2-way ANOVA (with overall p<0.001) and Bonferroni post-hoc tests compared to the respective infection control.

## SUPPLEMENTAL RESULTS

### Antibiotic capture by bacterial lipocalins uncovers an extracellular mechanism of intrinsic antibiotic resistance

Omar M. El-Halfawy<sup>a,b</sup>, Javier Klett<sup>c</sup>, Rebecca J. Ingram<sup>d</sup>, Slade A. Loutet<sup>e</sup>, Michael E. P. Murphy<sup>e</sup>,  
Sonsoles Martín-Santamaría<sup>c</sup>, and Miguel A. Valvano<sup>a,d,1</sup>

**X-ray crystallography and SEC-MALS.** BCNs generally consist of an extended, eight-stranded, antiparallel  $\beta$ -barrel with a lipocalin fold, able to host lipophilic ligands inside a lipophilic tunnel, together with a characteristic  $\alpha$ -helix (1). The crystal structure of BcnA was solved to 1.4 Å resolution in space group  $P6_1$  (Table S1). The asymmetric unit contained two molecules of BcnA. Recombinant BcnA lacked the predicted signal peptide (first 26 amino acids) of the full-length protein. In both chains, the model contained N-terminal histidyl and methionyl residues encoded from the expression plasmid, residues D27 through T185 of BcnA; only the terminal amino acid (K186) was not modeled. There are few contacts between the two protein chains in the asymmetric unit. The PDBePISA server (2) predicted that the molecules in the asymmetric unit are monomers in solution. The oligomeric solution state of BcnA was assessed using SEC-MALS. Recombinant BcnA, after cleavage of the 6X-His tag, has a predicted molecular mass of 17.4 kDa. The measured mass of BcnA in solution was 18 kDa (Fig. S4D). Based on these results we concluded that BcnA is a monomeric protein (Fig. 4A). Within the interior cavity of BcnA, continuous density was observed with a shape similar to that observed for isoprene-based molecules identified in homologous BCN structures (PDB IDs 1Y0G, 3Q34, 2X32, 2X34, 1WUB). We have modeled this density as octaprenyl pyrophosphate (OTP) (Fig. S4A) as observed in other BCN proteins after recombinant expression in *E. coli* (3, 4). Unambiguous density for the isoprene chain of OTP is observed in the BcnA structure; however, little density is present corresponding to the pyrophosphate portion of OTP. The isoprene tail of OTP makes numerous hydrophobic contacts with amino acid side chains located inside the BcnA barrel. The binding of these lipophilic ligands to the BCN homologues is likely due to recombinant expression in *E. coli*; hence these molecules might not be predictive of the functions of these BCN homologues.

The crystal structure of BcnB was solved to 1.6 Å resolution in space group  $P2_1$  (Table S1) with four molecules of BcnB in the asymmetric unit. Recombinant BcnB lacked a predicted signal peptide (first 22 amino acids) of the full-length protein. For chains B, C, and D, residues S24 to Q192 were modeled, while for chain A residues A25 to Q192 were modeled. All chains lack the C-terminal amino acid (Q193). PDBePISA predicted a stable dimer reconstructed through crystallographic symmetry that buries  $\sim 2840$  Å<sup>2</sup> of surface area, 15% of the solvent accessible surface area of each protomer. The mass of BcnB in solution was measured to be 38.1 kDa (Fig. S4E) by SEC-MALS. Recombinant BcnB, after cleavage of the 6X-His tag, has a predicted molecular mass of 19.2 kDa, indicating that BcnB is dimeric (Fig. 4B). Again, an interior of the cavity of BcnB contains continuous density that was modeled as OTP whose isoprene tail also makes numerous hydrophobic contacts with amino acid side chains located inside the BcnB barrel (Fig. S4B). In this case, the density supports both the isoprene chain and the pyrophosphate portions of OTP.

Structural alignments by the DALI server (5) indicated that both BcnA and BcnB were most similar to *E. coli* YceI (PDB ID 1Y0G). For BcnA, 156 residues were aligned (24% sequence identity) with a root mean squared deviation (rmsd) of 1.5 Å. For BcnB, 165 residues were aligned (33% sequence identity) with a

rmsd of 1.7 Å. BcnA and BcnB also shared structural similarity ( $Z$ -score  $> 3.0$ ) to eukaryotic lipocalins such as porcine odorant binding protein (PDB ID 1DZM) and plasma retinol-binding protein (PDB ID 1KT6), as well as avidin (PDB ID 2A5C). These results confirm that despite low sequence identity, BcnA and BcnB are members of the BCN family and both possess a lipocalin fold. A structural alignment of BcnA and BcnB (Fig. 4C) shows that the overall folds are very similar (148 residues aligned with an rmsd value of 1.66 Å) despite only sharing 22% sequence identity. The largest structural differences in the proteins are in two of loops at the open ends of the  $\beta$ -barrels. In BcnB these form a longer tunnel with amino acid residues extending past the OTP pyrophosphate (Fig. S4B), while in BcnA the OTP pyrophosphate extends past the end of the protein barrel. BcnB residues H42, W49, S84 (*via* a water-bridge), and K86 provide a hydrogen bonding network for the OTP pyrophosphate (Fig. S4C), while BcnA does not provide such a network.

**Extended computational studies of BcnA, BcnB, and complexes with the studied ligands.** We conducted structure-function analyses of BcnA to propose a plausible binding mode for antibiotics. The stability of the BcnA and BcnB models was tested by running 20 ns of molecular dynamics (MD) simulations with AMBER 12 (<http://ambermd.org/>). RMSD deviations and RMS fluctuations (Fig. S9a-b) show that the two systems reach stability along the MD simulation.

Docking of antibiotics in addition to Nile Red and  $\alpha$ -tocopherol was performed in the BcnA X-Ray structure, and binding poses were predicted. In addition, flexibility of the protein was also taken into account by allowing some residues to be flexible during the docking calculations. Docking results are shown for BcnA in Fig. 4D-E and Fig. S4F-I. Interestingly, two distinct binding modes were predicted for BcnA: antibiotics were predicted to bind at the rim of the lipocalin pocket whereas more lipophylic molecules such as Nile Red bind deeper inside the lipophylic tunnel.

All tested antibiotics shared ionic interactions with several polar residues, mainly K40, T46, D82, Q88, Y85, D93, and E165 (Fig. 4D and Fig. S4F-I). In addition to ionic interactions, other interactions were observed between the aromatic moieties present in PmB, rifampicin, norfloxacin, and ceftazidime, and lipophylic residues such as I171, Y85, M42, M84, V89, W94 and W166. Gentamicin does not possess any aromatic moieties, matching with its weak binding to BcnA. However, the inability to bind BcnA cannot be correlated exclusively to the absence of aromatic moieties; other factors such as entropic effects from solvation and/or conformational factors may be involved.

Docking calculations of Nile Red and the fat-soluble  $\alpha$ -tocopherol led to the prediction of the ligand deeply binding inside the lipophylic tunnel, establishing lipophylic interactions. In case of Nile Red, we predicted two alternative binding modes in BcnA, one with the diethylamino group pointing towards the entrance of the pocket, and other one with the diethylamino group pointing towards the interior of the protein. In the case of  $\alpha$ -tocopherol, it was found to be mainly docked with the alkyl chain buried into the pocket and the cyclic head placed towards the entrance of the pocket (Fig. 4E). The OH group from the chromanol head was not found to establish any preferred polar interaction over the different predicted poses.

BcnA model and docking calculations suggested D82 and D93 as important residues for the structure and function of BcnA. We found that in the wild type BcnA, the D82 carboxylate group establishes stable hydrogen bonds with the backbone NH groups of M84 and Y85 from helix D82-A89, and D93 carboxylate group establishes a stable hydrogen bond with the side chain OH group of T163. Prompted by this finding, we modeled the BcnA D82A-D93A mutant from the crystallographic structure, and submitted to MD simulations. The stability of the BcnA D82A-D93A double mutant model was tested by running 20 ns of MD simulation with AMBER 12. RMSD deviations and RMS fluctuations (Fig. S6A-B) show that the system reached stability along the MD simulation. We could only observe a slight lower fluctuation in the case of BcnA D82A-D93A mutant: a 3 Å of RMS fluctuation is reached in the region of the V38-E47 loop in the case of the D82A-D93A mutant while, in the case of the WT BcnA, a 4 Å of RMS fluctuation is

observed for the same loop, in accordance with the B-factors extracted from the crystallography structures. By contrast, in the case of the MD simulation of the BcnB, the equivalent F38-R50 loop showed a 2 Å of RMS fluctuation. To study the reason that causes this lower fluctuation in the BcnA mutant model, we inspected the MD simulations in detail. A higher mobility of the atoms belonging to the V38-E47 loop was found in the case of the wild type, as deduced from the RMS fluctuations of each residue (Fig. S6A-B). We observed that, in the case of the BcnA D82A-D93A mutant, the V38-E47 loop created new interactions between the backbone of M42 and S170, and Q41 and A173, maybe thus explaining this lower fluctuation.

In the D82A-D93A mutant, the absent carboxylate group of D82 is replaced by the backbone CO group from A82, allowing the hydrogen bonding to NH groups from M84 and Y85. This new situation might affect the overall BcnA structure and, very likely, the binding of antibiotics since D82 has been identified by our docking calculations as an important residue for antibiotic anchorage. Furthermore, in the case of D93 mutation, the absence of the hydrogen bond between the carboxylate group and the T163 side chain is not replaced by other equivalent interaction, allowing the approach of T163-I171 loop towards the V38-E47 loop, leading to two novel hydrogen bonds: one between the M42 NH group and the S170 CO group, and another one between the Q41 CO group and the A173 NH group (Fig. S6C-E). Together, this relatively different arrangement for the BcnA D82A-D93A mutant led to a reduced flexibility of the V38-E47 loop along the MD simulation time (Fig. S6C-E). The higher mobility of this V38-E47 loop could resemble the required movement of a similar loop in other member of the lipocalin family (the lipocalin type prostaglandin D synthase), where the conformational change of the Y107-S114 loop allows the change between the open/closed conformers (6). Nevertheless, the higher flexibility observed for the wild type structure could account for a better ability to bind ligands. Taking always into account the limitation of working with computational simulations, these observed changes might point out to a structural role for D82 and D93, in addition to their putative functional role in the binding of the antibiotics. To further investigate the role of these two residues, site-directed mutants with alanine replacements of these residues were prepared. D82 and to a less extent D93 were demonstrated to be important for the binding interaction of ligands (exemplified by Nile Red) to BcnA (Fig. S5A-B). Docking of Nile Red and  $\alpha$ -tocopherol into the BcnA D82A-D93A mutant (by following the general docking protocol with the minimized average structure from the ns 2.5 to the ns 5 of the MD simulation) did not lead to any binding pose inside the lipophilic tunnel. This agrees with the experimental results obtained with the BcnA D82A-D93A mutant protein.

Since BCNs are highly conserved among bacteria sharing the characteristic lipocalin tertiary structure, we determined the consensus motif of this protein family (Fig. S5C) (7). The D93 residue of BcnA of *B. cenocepacia* was highly conserved. Aspartate residues at distance from D93 comparable to the distance to D82 in *B. cenocepacia* BcnA were found in the motif (7). Together, this suggests that D82 and D93 may have a structural role to maintain the 3D structure and the opening of the lipophilic tunnel of BcnA, and also they may be proposed as key residues to interact with antibiotics, thus playing an essential role in the resistance mechanism mediated through BCNs. This mode of interaction between BCN and antibiotics could be common among this large family of conserved bacterial proteins.

1. **Bishop RE.** 2000. The bacterial lipocalins. *Biochim Biophys Acta* **1482**:73-83.
2. **Krissinel E, Henrick K.** 2007. Inference of macromolecular assemblies from crystalline state. *J Mol Biol* **372**:774-797.
3. **Handa N, Terada T, Doi-Katayama Y, Hirota H, Tame JR, Park SY, Kuramitsu S, Shirouzu M, Yokoyama S.** 2005. Crystal structure of a novel polyisoprenoid-binding protein from *Thermus thermophilus* HB8. *Protein Sci* **14**:1004-1010.

4. **Vincent F, Molin DD, Weiner RM, Bourne Y, Henrissat B.** 2010. Structure of a polyisoprenoid binding domain from *Saccharophagus degradans* implicated in plant cell wall breakdown. *FEBS Lett* **584**:1577-1584.
5. **Holm L, Rosenström P.** 2010. Dali server: conservation mapping in 3D. *Nucleic Acids Res* **38**:W545-549.
6. **Kumasaka T, Aritake K, Ago H, Irikura D, Tsurumura T, Yamamoto M, Miyano M, Urade Y, Hayaishi O.** 2009. Structural basis of the catalytic mechanism operating in open-closed conformers of lipocalin type prostaglandin D synthase. *J Biol Chem* **284**:22344-22352.
7. **Frith MC, Saunders NF, Kobe B, Bailey TL.** 2008. Discovering sequence motifs with arbitrary insertions and deletions. *PLoS Comput Biol* **4**:e1000071.

**Table S1. X-ray crystallography data collection and refinement statistics**

Parameter	BcnA	BcnB
<b>Data Collection*</b>		
Resolution Range (Å)	35.9 - 1.4 (1.43 – 1.4)	37.3 - 1.6 (1.63 – 1.6)
Space Group	$P6_1$	$P2_1$
Unit cell dimension (Å)	$a = 93.97, b = 93.97, c = 76.66, \gamma = 120^\circ$	$a = 51.2, b = 101.2, c = 63.5, \beta = 97.2^\circ$
Unique Reflections	75,559 (4,004)	82,019 (3,495)
Completeness (%)	99.9 (99.4)	97.3 (78.7)
CC1/2	0.999 (0.829)	0.997 (0.892)
Average $I/\sigma I$	17.1 (3.0)	11.3 (3.3)
Redundancy	10.5 (5.7)	3.8 (3.1)
$R_{merge}$	0.061 (0.492)	0.056 (0.265)
<b>Refinement</b>		
$R_{work}$ ( $R_{free}$ )	0.156 (0.183)	0.158 (0.192)
Number of water molecules	274	482
Overall $B$ -factor (Å <sup>2</sup> )	28.4	17.1
r.m.s.d.		
Bond lengths (Å)	0.01	0.025
Bond angles (°)	1.46	2.44
Ramachandran Plot (%)		
In most favorable	96.0	96.9
In disallowed	0.3	0.8

\*Data collection statistics in parentheses represent the highest resolution shells. Coordinates for the X-ray crystal structures of BcnA and BcnB have been deposited to the Protein Data Bank with Accession Codes 5IXH and 5IXG, respectively.

**Table S2. Strains and Plasmids**

Strain or plasmid	Relevant characteristics <sup>a</sup>	Source and/or reference
<b>Strains</b>		
<b><i>Burkholderia cenocepacia</i></b>		
K56-2	ET12 clone related to J2315, CF clinical Isolate	<sup>b</sup> BCRRC, (1)
OME19	K56-2 pSCrhaB2; Tp <sup>R</sup>	(2)
OME37	K56-2 pOE12; BCAL3310 with C-terminus FLAG tag; Tet <sup>R</sup>	This study
OME40	K56-2 pOE13; BCAL3311 with C-terminus FLAG tag; Tet <sup>R</sup>	This study
OME60	K56-2, <i>P<sub>BCAL3310</sub>::pGSVTp-luxCDABE</i> ; Tp <sup>R</sup>	This study
OME61	K56-2, <i>P<sub>BCAL3312-3311</sub>::pGSVTp-luxCDABE</i> ; Tp <sup>R</sup>	This study
OME62	K56-2, ΔBCAL3311	This study
OME65	K56-2, ΔBCAL3310	This study
OME66	K56-2 pDA17; Tet <sup>R</sup>	This study
OME71	OME62 pSCrhaB2; Tp <sup>R</sup>	This study
OME72	OME62 pOE33 (BCAL3311); Tp <sup>R</sup>	This study
OME73	OME62 pOE34 (PA0423); Tp <sup>R</sup>	This study
OME74	OME62 pOE35 (PA4340); Tp <sup>R</sup>	This study
OME75	OME62 pOE36 (PA4345); Tp <sup>R</sup>	This study
OME76	OME62 pOE37 (Rv1890c); Tp <sup>R</sup>	This study
OME77	OME62 pOE38 (SAUSA300_2620); Tp <sup>R</sup>	This study
<b><i>Escherichia coli</i></b>		
DH5α	F <sup>+</sup> φ80 <i>lacZ</i> M15 <i>endA1 recA1 supE44 hsdR17</i> (r <sub>K</sub> <sup>-</sup> m <sub>K</sub> <sup>+</sup> ) <i>deoR thi-1 nupG supE44 gyrA96relA1</i> Δ( <i>lacZYA-argF</i> ) <i>U169</i> , λ-	Laboratory stock
GT115	F <sup>-</sup> <i>mcrA</i> Δ( <i>mrr-hsdRMS-mcrBC</i> ) φ80Δ <i>lacZ</i> ΔM15 Δ <i>lacX74 recA1 rpsL</i> (StrA) <i>endA1</i> Δ <i>dcm uidA</i> (ΔMluI):: <i>pir-116</i> Δ <i>sbcC-sbcD</i>	Invivogen, San Diego, CA
BL21	F <sup>-</sup> <i>dcm ompT hsdS</i> (r <sub>B</sub> <sup>-</sup> m <sub>B</sub> <sup>-</sup> ) <i>gal</i>	Novagen
<b><i>Pseudomonas aeruginosa</i></b>		
PAO1	Non-CF clinical isolate	(3)
Q502	CF clinical isolate	(4)
<b><i>Salmonella typhi</i></b>		
SARB63		(5)
<b><i>Shigella flexneri</i></b>		
SF51571	Serotype 1a, antigenic formula 1:4	Laboratory stock
<b><i>Acinetobacter</i> species</b>		
<i>A. baumannii</i> (AB1)	Clinical isolate	LHSC <sup>c</sup>
<i>A. lwoffii</i> (AB2)	Clinical isolate	LHSC <sup>c</sup>
<i>A. junii</i> (AB3)	Clinical isolate	LHSC <sup>c</sup>



***Klebsiella pneumoniae***

Kpn18	Clinical isolate	Laboratory stock
-------	------------------	------------------

***Staphylococcus aureus***

USA300	Community acquired MRSA	Martin McGavin
--------	-------------------------	----------------

**Plasmids**

pRK2013	<i>ori<sub>colE1</sub></i> , RK2 derivative, Kan <sup>R</sup> , <i>mob</i> <sup>+</sup> , <i>tra</i> <sup>+</sup>	(6)
pGSVTp- <i>lux</i>	Mobilizable suicide vector containing <i>lux</i> operon, derivative from pGSV3- <i>lux</i> (7); OriT; Tp <sup>R</sup>	(8)
pSCrhaB2	<i>ori<sub>pBBR1</sub></i> <i>rhaR</i> , <i>rhaS</i> , <i>P<sub>rhaB</sub></i> Tp <sup>R</sup> <i>mob</i> <sup>+</sup>	(9)
pDAI-SceI-SacB	<i>ori<sub>pBBR1</sub></i> , Tet <sup>R</sup> , <i>P<sub>dhfr</sub></i> , <i>mob</i> <sup>+</sup> , expressing I-SceI, SacB	(10)
pGPI-SceI	<i>ori<sub>R6K</sub></i> , ΩTp <sup>R</sup> , <i>mob</i> <sup>+</sup> , including an I-SceI restriction site	(11)
pDA17	<i>ori<sub>pBBR1</sub></i> , Tet <sup>R</sup> , <i>mob</i> <sup>+</sup> , <i>P<sub>dhfr</sub></i> , FLAG epitope	D. Aubert, unpublished
pOE12	pDA17, BCAL3310, C-terminus FLAG, Tet <sup>R</sup>	This study
pOE13	pDA17, BCAL3311, C-terminus FLAG, Tet <sup>R</sup>	This study
pOE15	BCAL3310 without signal peptide encoding sequence cloned in pET28a(+)	(2)
pOE16	BCAL3311 without signal peptide encoding sequence cloned in pET28a(+)	(2)
pOE22	<i>P<sub>BCAL3310::luxCDABE</sub></i> transcriptional fusion in pGSVTp- <i>lux</i> , Tp <sup>R</sup>	This study
pOE23	<i>P<sub>BCAL3312-3311::luxCDABE</sub></i> transcriptional fusion in pGSVTp- <i>lux</i> , Tp <sup>R</sup>	This study
pOE25	pGPI-SceI with fragments flanking BCAL3310, Tp <sup>R</sup>	This study
pOE26	pGPI-SceI with fragments flanking BCAL3311, Tp <sup>R</sup>	This study
pOE33	pSCrhaB2, BCAL3311, Tp <sup>R</sup>	This study
pOE34	pSCrhaB2, PA0423, Tp <sup>R</sup>	This study
pOE35	pSCrhaB2, PA4340, Tp <sup>R</sup>	This study
pOE36	pSCrhaB2, PA4345, Tp <sup>R</sup>	This study
pOE37	pSCrhaB2, Rv1890c, Tp <sup>R</sup>	This study
pOE38	pSCrhaB2, SAUSA300_2620, Tp <sup>R</sup>	This study
pOE39	pOE16, D82A	This study
pOE41	pOE16, D93A	This study
pOE46	pOE39, D93A	This study

<sup>a</sup>Tp<sup>R</sup>, trimethoprim resistance, Kan<sup>R</sup>, kanamycin resistance, Tet<sup>R</sup>, tetracycline resistance.

<sup>b</sup>BCRRC, *B. cepacia* Research and Referral Repository for Canadian CF Clinics.

<sup>c</sup>LHSC, London Health Science Centre, London, Ontario, Canada.

**TABLE REFERENCES**

1. Mahenthalingam E, Coenye T, Chung JW, Speert DP, Govan JR, Taylor P, Vandamme P. 2000. Diagnostically and experimentally useful panel of strains from the *Burkholderia cepacia* complex. J. Clin. Microbiol. **38**:910-913.

2. **El-Halfawy OM, Valvano MA.** 2013. Chemical communication of antibiotic resistance by a highly resistant subpopulation of bacterial cells. *PLoS One* **8**:e68874.
3. **Holloway BW.** 1955. Genetic recombination in *Pseudomonas aeruginosa*. *J Gen Microbiol* **13**:572-581.
4. **Camper N, Glasgow AM, Osbourn M, Quinn DJ, Small DM, McLean DT, Lundy FT, Elborn JS, McNally P, Ingram RJ, Weldon S, Taggart CC.** 2016. A secretory leukocyte protease inhibitor variant with improved activity against lung infection. *Mucosal Immunol* **9**:669-676.
5. **Boyd EF, Wang FS, Beltran P, Plock SA, Nelson K, Selander RK.** 1993. *Salmonella* reference collection B (SARB): strains of 37 serovars of subspecies I. *J Gen Microbiol* **139 Pt 6**:1125-1132.
6. **Figurski DH, Helinski DR.** 1979. Replication of an origin-containing derivative of plasmid RK2 dependent on a plasmid function provided in *trans*. *Proc Natl Acad Sci USA* **76**:1648-1652.
7. **Moore RA, Reckseidler-Zenteno S, Kim H, Nierman W, Yu Y, Tuanyok A, Warawa J, DeShazer D, Woods DE.** 2004. Contribution of gene loss to the pathogenic evolution of *Burkholderia pseudomallei* and *Burkholderia mallei*. *Infect Immun* **72**:4172-4187.
8. **Bernier SP, Nguyen DT, Sokol PA.** 2008. A LysR-type transcriptional regulator in *Burkholderia cenocepacia* influences colony morphology and virulence. *Infect Immun* **76**:38-47.
9. **Cardona ST, Valvano MA.** 2005. An expression vector containing a rhamnose-inducible promoter provides tightly regulated gene expression in *Burkholderia cenocepacia*. *Plasmid* **54**:219-228.
10. **Hamad MA, Skeldon AM, Valvano MA.** 2010. Construction of aminoglycoside-sensitive *Burkholderia cenocepacia* strains for use in studies of intracellular bacteria with the gentamicin protection assay. *Appl Environ Microbiol* **76**:3170-3176.
11. **Flannagan RS, Linn T, Valvano MA.** 2008. A system for the construction of targeted unmarked gene deletions in the genus *Burkholderia*. *Environ. Microbiol.* **10**:1652-1660.